

Inversion of stellar statistics equation for the Galactic Bulge

M. López-Corredoira ^{★1}, P. L. Hammersley¹, F. Garzón^{1,2}, E. Simonneau³,
 T. J. Mahoney¹

¹ Instituto de Astrofísica de Canarias, E-38200 La Laguna, Tenerife, Spain

² Departamento de Astrofísica. Universidad de La Laguna, E-38204 La Laguna, Tenerife, Spain

³ Institut d’Astrophysique de Paris, F-75014 Paris, France

Accepted xxxx. Received xxxx; in original form xxxx

ABSTRACT

A method based on Lucy (1974) iterative algorithm is developed to invert the equation of stellar statistics for the Galactic bulge and is then applied to the K -band star counts from the Two-Micron Galactic Survey in a number of off-plane regions ($10^\circ > |b| > 2^\circ$, $|l| < 15^\circ$).

The top end of the K -band luminosity function is derived and the morphology of the stellar density function is fitted to triaxial ellipsoids, assuming a non-variable luminosity function within the bulge. The results, which have already been outlined by López-Corredoira et al. (1997b), are shown in this paper with a full explanation of the steps of the inversion: the luminosity function shows a sharp decrease brighter than $M_K = -8.0$ mag when compared with the disc population; the bulge fits triaxial ellipsoids with the major axis in the Galactic plane at an angle with the line of sight to the Galactic centre of 12° in the first quadrant; the axial ratios are 1:0.54:0.33, and the distance of the Sun from the centre of the triaxial ellipsoid is 7860 pc.

The major–minor axial ratio of the ellipsoids is found not to be constant, the best fit to the gradient being $K_z = (8.4 \pm 1.7) \times \exp(-t/(2000 \pm 920) \text{ pc})$, where t is the distance along the major axis of the ellipsoid in parsecs. However, the interpretation of this is controversial. An eccentricity of the true density-ellipsoid gradient and a population gradient are two possible explanations.

The best fit for the stellar density, for $1300 \text{ pc} < t < 3000 \text{ pc}$, are calculated for both cases, assuming an ellipsoidal distribution with constant axial ratios, and when K_z is allowed to vary. From these, the total number of bulge stars is $\sim 3 \times 10^{10}$ or $\sim 4 \times 10^{10}$, respectively.

Key words: Galaxy: structure — infrared: stars — Galaxy: stellar content — stellar statistics

1 INTRODUCTION

This paper examines two aspects of the bulge: the luminosity function for the brightest stars in the K ($2.2 \mu\text{m}$) band and the density distribution of these stars.

There are many aspects of the bulge of the Galaxy that are still unknown, mainly because of the high extinction due to interstellar gas and dust. One of these unknowns is the near-infrared luminosity function, which has been principally derived from observations in Baade’s Window (Frogel & Whitford 1987; Davidge 1991; De Poy et al. 1993; Ruelas-Mayorga & Noriega-Mendoza 1995; Tiede et al. 1995). Gould (1997) and Holtzman et al. (1998) have used the *Hubble*

Space Telescope to study the V and I luminosity functions. However, extrapolations from Baade’s and other clear windows to the whole bulge may not be appropriate, in particular because these are ‘special’ regions. Furthermore, these regions are very small, containing relatively few stars, so they give very poor statistics at the brighter magnitudes. This bright end of the luminosity function is very important in order to determine the age of the population, for instance.

Many authors have found non-axisymmetry in the Galactic bulge[†] (Feast & Whitelock 1990) through the analysis of star counts (Nakada et al. 1991; Weinberg 1992;

[★] Electronic mail: martinlc@iac.es.

[†] Some authors call it the “bar” instead of the bulge. See, for instance, Gerhard, Binney & Zhao (1998).

Whitelock et al. 1991; Stanek et al. 1994, 1996; Woźniak & Stanek 1996) or integrated flux maps (Blitz & Spergel 1991; Weiland et al. 1994; Dwek et al. 1995; Sevenster 1996). This asymmetry has a negligible out-of-plane tilt (Weiland et al. 1994) and gives more counts in positive than in negative galactic longitudes. However, other authors (Ibata & Gilmore 1995; Minniti 1996) claim that axisymmetry is suitable. Besides the discussion about whether there is triaxiality or not, the actual shape and inclination of the bulge is also under debate with currently no clear agreement among different authors.

Traditionally, star counts have been interpreted by fitting parameters to the functions. An assumption of an a priori shape of the bulge is made, along with the characteristics of its population. Free parameters are then fitted to the data and the model is obtained. This is the usual way of extracting information concerning the different components of the Galaxy from star counts (Bahcall & Soneira 1980; Buser & Kaeser 1983; Prichet 1983; Gilmore 1984; Robin & Crézé 1986; Ruelas-Mayorga 1991; Wainscoat et al. 1992; Ortiz & Lépine 1993). The number of possible parameters to fit is limited to a priori assumptions about the shape (ellipsoidal, etc.) needed.

In general, surface brightness maps are also interpreted by fitting parameters (Dwek et al. 1995; Freudreich 1998). However, although these maps cover large areas, a brief examination of the equations shows that they give no information on the luminosity functions. Therefore, when making the fit to the bulge, the number of free parameters is very small and applies only to the density function. Even in Freudreich (1998), where in total some 30 parameters are used, only a very few of these apply to the bulge and only a very few parameters are solved at one go.

In this paper we examine the TMGS star counts between $m_K=4$ and 9 mag in 71 regions across the bulge. The counts for these regions are shown in Hammersley et al. (1999), where a qualitative discussion on the counts is presented. It is shown that the counts are highly asymmetric in longitude when compared with the predictions of a symmetric model.

Clearly, there is a relation between surface brightness and star counts as one is the integral of the other, but they are not the same or even similar and cannot be handled in the same manner. One way of looking at the difference between the two is to consider that at a single position a surface brightness map gives just a single value whilst star counts give a counts. vs magnitude plot. From this plot alone it is possible to determine things about the structure. Therefore, while star counts and surface brightness maps are clearly related, they behave very differently. Many authors, including ourselves, have already used the fitting approach to look at the surface brightness *COBE*-DIRBE data (we note that Binney et al. 1997 have tried inversions on the surface brightness maps), but this is not the best for star counts in the present situation.

One of the major advantages in analysing star counts as opposed to surface brightness maps is that the magnitude range can be limited in order to highlight the features of interest. This is of particular value when looking for triaxiality because if one region is significantly closer than another then, simply from the inverse square dependence with the distance, the sources from the further region are not de-

tected until a fainter magnitude. Hammersley et al. (1999) show that in the TMGS star counts the size of the asymmetry amounts to some 50% of the bulge counts in some magnitude ranges, in the *COBE*-DIRBE maps the asymmetry is far less. For this reason analysis of 2- μ m star counts in a certain magnitude range will be far more sensitive in determining the triaxiality of the bulge than surface brightness maps.

Whilst large-area star counts, as used here, contain far more information than surface brightness maps they are intrinsically far more difficult to analyse. *A priori*, neither is known and furthermore there is no reason to believe that the luminosity function (LF) is a simple analytical expression. Therefore, whereas fitting a surface brightness map there will only be a few free parameters, this is not the case for star counts. In this case the number of free parameters would rise unmanageably and so we would be forced to adopt *a priori* assumptions on the LF and density functions with the severe risk that the final result is dependent on these initial assumptions.

We have therefore chosen a different approach, that of direct inversion. Assumptions on the shape of the solution-functions (in this case, these are the luminosity function and the density of stars) are not made but instead come directly from the data by means of an ‘‘inversion’’ technique. Once the solutions for the functions are produced by the inversion, they are compared *a posteriori* to some known analytical expression (for instance, an ellipsoidal shape for the bulge isodensity contours) and, afterwards, fitted to them. This method allows all possible solutions to be examined, rather than solely that of the initial assumption and the only fitting are density contours to a density map. No attempt need to be made to fit a density function to the star counts.

Since the first decades of this century, attempts have been made to invert the star-count equation (eq. 1). However, problems such as excessive patchiness of extinction in optical star counts or instabilities of an ill-posed problem in the mathematical technique of inversion, hindered the development of the technique. In this paper the extinction problems are ameliorated by using the near-infrared K band and the instabilities by using a statistical iterative algorithm of inversion (Lucy 1974). A full explanation of the inversion is developed in this paper (with the core in §4) whose results have already been outlined by López-Corredoira et al. (1997b).

2 NEAR-INFRARED DATA

K -band star counts were taken from the Two Micron Galactic Survey (TMGS; Garzón et al. 1993, 1996), which covers about 350 deg² of sky and has detected some 700000 stars in or near the Galactic plane. This survey provides K -band observations of several regions that cross the Galactic plane, in the areas $-5^\circ < l < 35^\circ$, $|b| \leq 15^\circ$ and $35^\circ < l < 180^\circ$, $|b| \leq 5^\circ$.

Regions from three strips of constant declination are used (Table 1) In this study of the bulge. More specifically, 71 regions were selected from those strips in off-plane regions, but not too far from the Galactic centre ($10^\circ > |b| > 2^\circ$, $|l| < 15^\circ$). Each region has an area on the sky between 0.4 and 1.9 deg². The chosen regions are listed

Table 1. Constant-declination TMGS strip used in this paper.

$\delta_{\text{central}}(\text{J2000})$	Cut in the Galactic plane (deg)	Strip width ($\Delta\delta$) (deg)
$-29^{\circ}43'32''$	$l = -0.9$	2.51
$-22^{\circ}26'40''$	$l = 7.5$	1.63
$-15^{\circ}33'24''$	$l = 15.4$	0.78

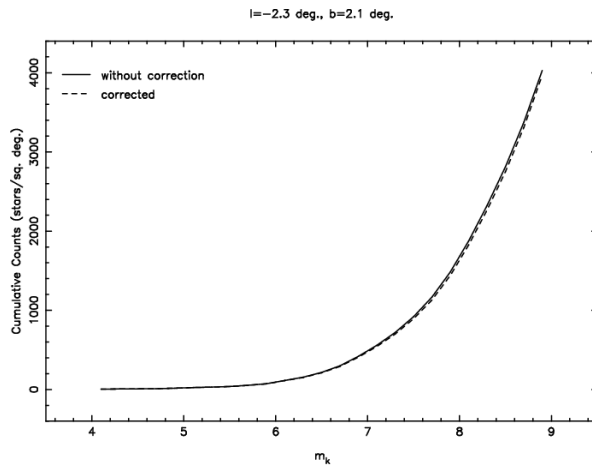


Figure 1. Comparison of cumulated star counts without confusion correction and those corrected according to the method explained in López-Corredoira et al. (1997a) with a linear extrapolation of the differential star counts over magnitude 9.4.

in Table 2. There is an overlap in the neighbouring regions such that some stars fall into two regions. The total covered area of sky covered is 75 deg^2 . This area is far greater than that used in Baade's window or any of the other low extinction region and hence provides much better statistics for the top end of the bulge LF.

The chosen regions contain principally bulge and disc stars. The area near the Galactic plane was not used in order to avoid components which belong neither to the bulge nor to the disc (e.g. spiral arms) and the high and variable extinction. The outer limits were set so that the bulge-to-disc stellar ratio was still acceptable, i.e. so that there were sufficient bulge stars in comparison with disc stars to make the study of the bulge meaningful..

The survey is complete between the magnitude limits $m_K = 4.0$ mag and $m_K \approx 9.2$ mag, except for the regions very near the Galactic centre where source confusion reduced the faint limit by about half a magnitude, although the detection limiting magnitude of the survey is in excess of 10 mag. Hence, inversion will be applied up to $m_K = 8.6$ mag for the regions of the strip with declination -30° and up to $m_K = 9.0$ mag for the remaining cases.

Figure 2 shows cumulative star counts, N , for the three strips up to $m_K = 9$ mag as a function of b (l also varies, as can be seen in Fig. 9).

Within this range of magnitudes, confusion effects are negligible. This was determined from the application of the method explained by López-Corredoira et al. (1997a) by assuming an extrapolation to fainter magnitudes (Fig. 1). As

can be seen in the figure, the counts are nearly the same with or without correction. That confusion is not significant for the areas chosen can also be seen in the figures in Hammerley et al. (1999) where the TMGS star counts are directly compared with the W92 model counts (Cohen 1994). Taking into account that the correction is based on an extrapolation and the changes are minor when compared to the other sources of error, it is preferable to avoid any correction and use the original counts.

3 THE STELLAR STATISTICS EQUATION FOR THE BULGE

3.1 Cumulative star counts

For each of the 71 regions centred on galactic coordinates $(l, b)_i$, where i is the field number, the cumulative star counts observed in a filter K , N_K , up to a magnitude m_K in a given region of solid angle ω is the sum of the stars over the beam with such an apparent magnitude (Bahcall 1986). Assuming a luminosity function which does not vary with the spatial position for each Galactic component c , this is

$$N_K(m_K)\omega \sum_c \int_0^\infty \Phi_{K,c}(m_K + 5 - 5 \log_{10} r - a_K(r)) \times D_c(r)r^2 dr, \quad (1)$$

where

$$\Phi_{K,c}(M_K) = \int_{-\infty}^{M_K} \phi_{K,c}(M)dM, \quad (2)$$

$\phi_{K,c}$ is the normalized luminosity function for the K band in the component c ; D_c is the density function in the component c and $a_K(r)$ is the extinction along the line of sight for the K band.

3.2 Extinction

If the star counts, N_K , for eq. (1), and the luminosity function, $\phi_{K,c}$, are known then the densities and the extinction would be the unknown functions. The extinction can be separated from the last integral equation by means of a suitable change of variable (Bok 1937; Trumpler & Weaver 1953; Mihalas & Binney 1981, ch. 4):

$$\rho_K = 10^{0.2a_K(r)}r, \quad (3)$$

$$\Delta_{c,K}[\rho_K(r)] = \frac{D_c(r)}{\left(1 + 0.2(\ln 10)r \frac{da_K(r)}{dr}\right) 10^{0.6a_K(r)}}, \quad (4)$$

which transforms the stellar statistics equation into

Table 2. The regions whose star counts are used to invert and extract information about the bulge.

l (deg)	b (deg)	Area (deg 2)	l (deg)	b (deg)	Area (deg 2)	l (deg)	b (deg)	Area (deg 2)
-6.3	7.8	0.4	2.6	-6.1	1.9	9.0	-2.7	1.4
-5.7	7.1	0.8	3.0	-6.9	1.9	9.1	-2.9	1.4
-5.2	6.4	1.3	3.4	-7.7	1.8	9.2	-3.0	1.4
-4.7	5.7	1.8	3.8	-8.5	1.8	9.6	-3.9	1.4
-4.2	5.0	1.9	4.2	-9.2	1.8	10.1	-4.7	1.4
-3.7	4.3	1.9	1.3	9.9	1.4	10.5	-5.5	1.4
-3.2	3.5	1.9	1.8	9.1	1.4	10.9	-6.3	1.4
-2.7	2.8	1.9	2.3	8.4	1.4	11.3	-7.1	1.4
-2.6	2.7	1.9	2.9	7.6	1.4	11.7	-8.0	1.4
-2.5	2.5	1.9	3.4	6.8	1.4	12.2	-8.8	1.4
-2.4	2.4	1.9	3.9	6.0	1.4	12.6	-9.6	1.4
-2.3	2.2	1.9	4.4	5.3	1.4	9.7	9.9	0.7
-2.3	2.1	1.9	4.9	4.5	1.4	10.2	9.1	0.7
0.3	-2.0	1.9	5.4	3.7	1.4	10.7	8.3	0.7
0.4	-2.2	1.9	5.8	2.9	1.4	11.2	7.4	0.7
0.5	-2.3	1.9	5.9	2.7	1.4	11.7	6.6	0.7
0.6	-2.5	1.9	6.0	2.6	1.4	12.2	5.8	0.7
0.7	-2.6	1.9	6.1	2.4	1.4	12.6	4.9	0.7
0.7	-2.8	1.9	6.2	2.3	1.4	13.1	4.1	0.7
0.8	-2.9	1.9	6.3	2.1	1.4	13.6	3.3	0.7
0.9	-3.1	1.9	8.7	-2.1	1.4	14.1	2.4	0.7
1.3	-3.9	1.9	8.8	-2.2	1.4	14.2	2.2	0.7
1.8	-4.6	1.9	8.9	-2.4	1.4	14.3	2.1	0.7
2.2	-5.4	1.9	8.9	-2.6	1.4			

$$N_K(m_K) = \omega \sum_c \int_0^\infty \Phi_{K,c}(m_K + 5 - 5 \log_{10} \rho_K) \times \Delta_{c,K}(\rho_K) \rho_K^2 d\rho_K. \quad (5)$$

The functions $\Delta_{c,K}(\rho_K)$ do not have a direct physical meaning but are fictitious densities as a function of a fictitious distance which coincides with the real distance only when there is no extinction (see Calbet et al. 1995).

For the extinction we have followed Wainscoat et al. (1992, hereafter W92), who assume that the extinction has an exponential distribution with the same scale length as the old disc, 3.5 kpc, and a scale height of 100 pc. This is normalized to give $A_K = da_K/dr = 0.07$ mag kpc $^{-1}$ in the solar neighbourhood. Although this model is crude it is sufficient for our purposes. As the areas of interest are off the plane, the extinction in the direction of the bulge sources is between 0.05 to 0.5 mag at K (ten times lower than in V). The evidence from the 2.2- μ m surface brightness maps is that there are off-plane clouds, but these are isolated so if a strip did cross a cloud it would affect only one or two regions which would have a minor effect on the final result. In fact, Hammersley et al. (1999) show that in the regions chosen there are no major dips in the counts and hence no isolated clouds. Furthermore, in this paper there is a discussion on the IR extinction in the plane and comparison is made with the W92 model, which uses the above model for the extinction. It is shown that in the solar neighbourhood this model works well and remains valid to a galactocentric distance of about 4 kpc where the molecular ring is situated. Inside the ring the extinction is then over estimated. However, it should be noted that for the lines of sight used here the majority of the extinction occurs in the first few kpc, i.e. while the line of sight is close to the Galactic plane. There-

fore, the extra extinction added by the model in the inner galaxy is a small proportion of the total extinction along the line of sight, which is in turn already small. This effect is clearly demonstrated by Hammersley et al (1999) for the $l = 7^\circ$ strip where the effect of the overestimated extinction can only be seen within 0.5° of the plane.

Another possible cause for concern could be if there was a general asymmetry in the extinction, either from above to below the plane or between positive and negative longitudes. However, it must be noted that the analysis of Freudreich (1998) of the COBE-DIRBE surface brightness maps shows no such asymmetry. Furthermore, Hammersley et al. (1999) have analysed the asymmetry in the TMGS bulge star counts and show that the form is not consistent with the asymmetry being caused by extinction. Therefore, although the extinction model is crude it is valid for the purpose used here.

So, from a_K , the relationship is obtained between Δ —the fictitious density— and D —the real density— for each component, using eq. (3); therefore eq. (5) will be used hereafter.

3.3 Subtraction of the disc

The components cannot all be solved simultaneously and the inversion of eq. (5) can only be solved when the number of components, c , is restricted to one.

It will be assumed that, in the chosen regions, the contribution to the star counts will be primarily from the disc and bulge. In order to isolate the bulge component, therefore, the contribution of the disc must be subtracted from the total counts for each region.

The model of the disc coded by us was based on W92,

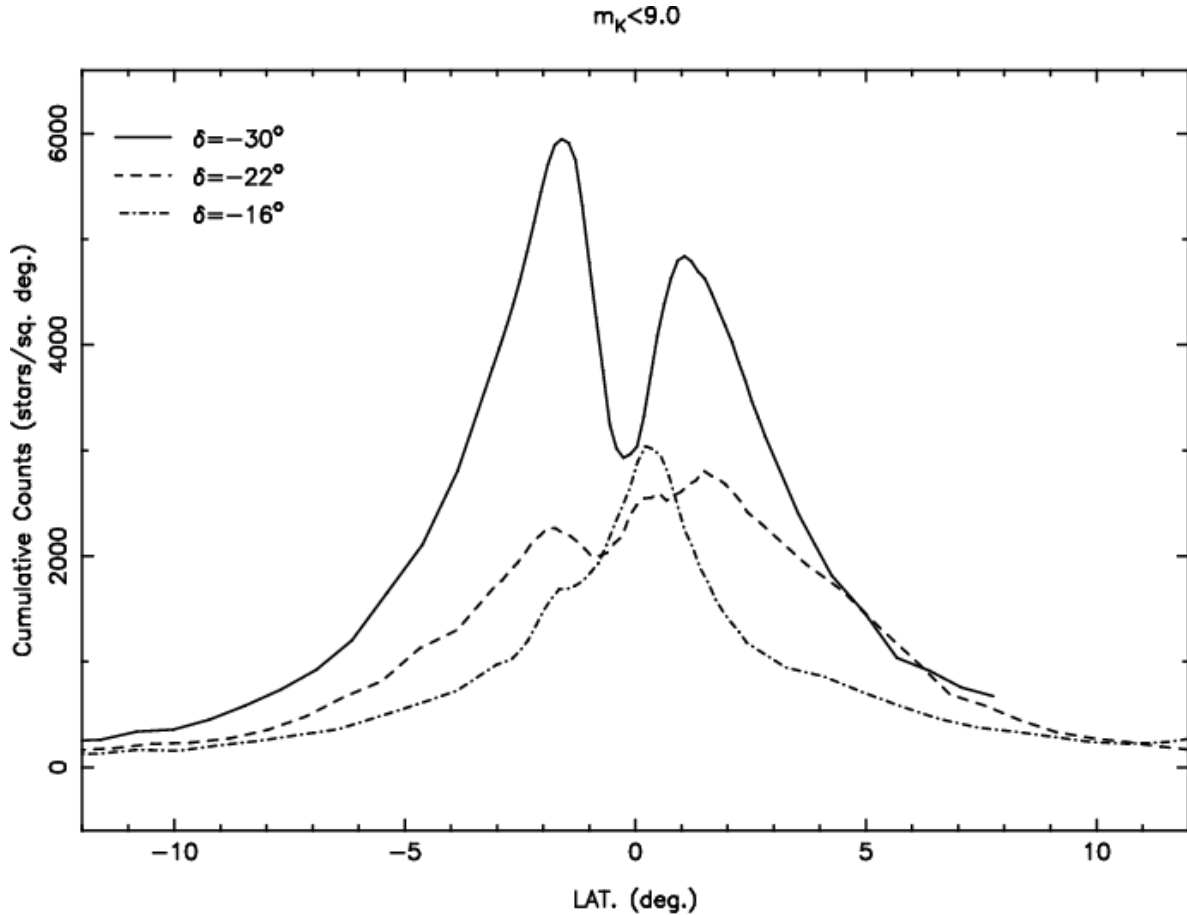


Figure 2. $N(m_K = 9.0 \text{ mag})$ along the three strips that are used with constant declinations: $\delta = -30^\circ$, which cuts the plane at $l = -1^\circ$; $\delta = -22^\circ$, which cuts the plane at $l = 7^\circ$; and $\delta = -16^\circ$, which cuts the plane at $l = 15^\circ$.

which follows Bahcall & Soneira (1980). It has been used because it provides a good fit to the TMGS counts in the region where the disc dominates (Cohen 1994b; Hammersley et al. 1999). The W92 model was revised by Cohen (1994a) but this does not significantly alter the form of the disc in the areas of interest. Three examples of those fits are shown in Fig. 3, in regions where the disc is isolated (note that the regions used in these plots are different from the regions used for the inversion specified in §2). A more detailed comparison of the W92 model and the TMGS is presented by Hammersley et al. (1999), who examine some 300 square degrees of sky. Hence, by extrapolation, it is expected that this disc model will adequately reflect the disc components along the lines of sight used in this paper. Initially, it was also expected that the W92 model would give an adequate fit for the bulge counts; this, however, was not the case as can be clearly seen in Hammersley et al. (1999).

3.4 Fredholm integral equations of the first kind

Once the disc star counts are subtracted, a Fredholm integral equation of the first kind is derived (see Trumpler & Weaver 1953):

$$N_{K,\text{bulge}}(m_K) = N_K(m_K) - N_{K,\text{disc}}(m_K)$$

$$= \omega \int_0^\infty \Phi_{K,\text{bulge}}(m_K + 5 - 5 \log_{10} \rho_K) \Delta_{\text{bulge},K}(\rho_K) \times \rho_K^2 d\rho_K, \quad (6)$$

where Δ is the unknown function and Φ is the kernel of the integral equation.

When Φ is the unknown function instead of Δ , then a new change of variable can be made: $M_K = m_K + 5 - 5 \log_{10} \rho_K$, and a new Fredholm equation of the first kind is obtained:

$$N_K(m_K) = 200(\ln 10)10^{\frac{3m_K}{5}} \times \int_{-\infty}^\infty \Delta_K(10^{\frac{5+m_K-M_K}{5}})10^{\frac{-3M_K}{5}} \Phi_K(M_K) dM_K. \quad (7)$$

In this case, the kernel is Δ instead of Φ . Any method of inverting eq. (6) is also applicable to this integral equation (7).

4 INVERSION OF THE STELLAR STATISTICS EQUATION

The inversion of integral equations such as (6) or (7) is ill-conditioned. Typical analytical methods for solving these equations (see Balázs 1995) cannot achieve a good solution

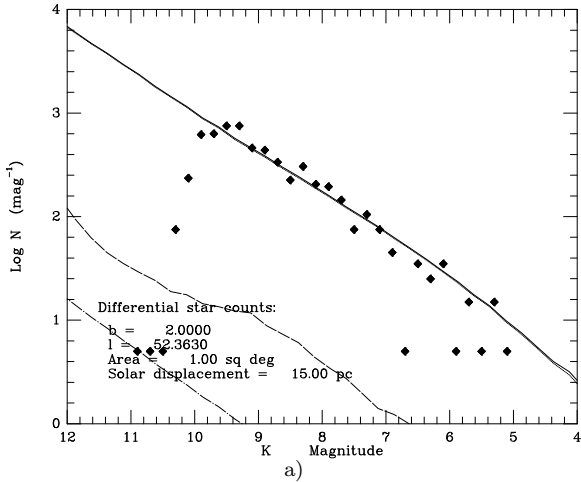
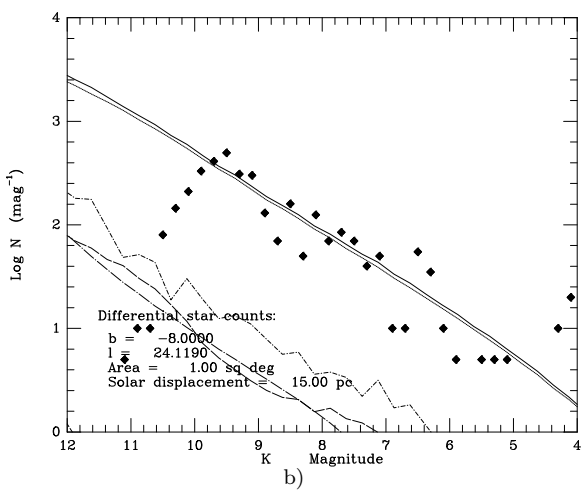


Figure 3. Differential star counts, the derivative of the cumulative star counts. Rhombi are TMGS data. Lines represent the W92 model: the solid line stands for counts for all components; the dotted line stands for disc counts; long-dashed line for spiral arms; short-dashed and dotted line for the ring; shot-dashed line for the bulge; long-dashed and dotted line for the halo. In these cases - a), b) and c) - disc and total counts are nearly coincident because the disc gives the most part of the stars.

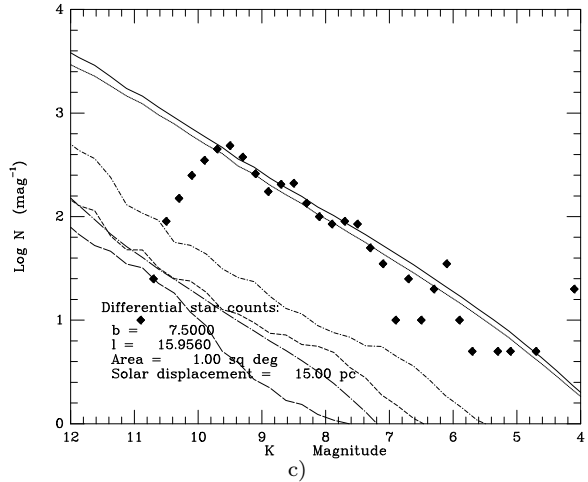


because of the sensitivity of the kernel to the noise of the counts (see, for instance, Craig & Brown 1986, ch. 5).

Since the functions in these equations have a stochastic rather than analytical interpretation, it is to be expected that statistical inversion algorithms will be more robust. This is confirmed by several authors, for instance Turchin et al. (1971), Jupp et al. (1975), Baláz (1995).

From among these statistical methods, we have selected Lucy's algorithm (Lucy 1974; Turchin et al. 1971; Baláz 1995), an iterative method, the key to which is the interpretation of the kernel as a conditioned probability and the application of Bayes' theorem[†].

[†] Bayesian methods have multiple applications in astrophysics. Inversion problems are particular cases of these applications (Loredo 1990).



In eq. (6), Δ is the unknown function, and the kernel is Φ , which depends on the apparent magnitude conditioned to the fictitious distance ρ . The fictitious density Δ can also be understood in terms of a probability density (the probability of finding a star with fictitious distance ρ). Thus, eq. (6) can be rewritten as (hereafter, the notation for component or passband will be dropped)

$$N(m) = \int_0^\infty \Delta(\rho) P(m|\rho) d\rho, \quad (8)$$

where

$$P(m|\rho) = \rho^2 \Phi(m + 5 - 5 \log_{10} \rho). \quad (9)$$

The inverse conditioned probability, i.e. the probability of star being at a fictitious distance ρ , once its apparent magnitude m is known, is given by Bayes' theorem:

$$Q(\rho|m) = \frac{\Delta(\rho) P(m|\rho)}{\int_0^\infty \Delta(x) P(m|x) dx}. \quad (10)$$

From the definition of conditioned probability,

$$\Delta(\rho) P(m|\rho) = N(m) Q(\rho|m), \quad (11)$$

and, hence, we get directly:

$$\Delta(\rho) = \frac{\int_{m_{\min}}^{m_{\max}} dm N(m) Q(\rho|m)}{\int_{m_{\min}}^{m_{\max}} dm P(m|\rho)}. \quad (12)$$

Equations (12) and (10) together lead to an iterative method[§] of obtaining the unknown function $\Delta(\rho)$:

$$\Delta^{r+1}(\rho) = \Delta^r(\rho) \frac{\int_{m_{\min}}^{m_{\max}} \frac{N^{\text{obs}}(m)}{N^r(m)} P(m|\rho) dm}{\int_{m_{\min}}^{m_{\max}} P(m|\rho) dm}, \quad (13)$$

where N^{obs} represents the observed cumulative counts and

$$N^r(m) = \int_0^\infty \Delta^r(x) P(m|x) dx. \quad (14)$$

[§] For the numerical calculation of these integrals ρ is placed into discrete logarithmic intervals (the $(m, \log \pi)$ method; Mihalas & Binney 1981, ch. 4) in such a way that $\log_{10} \rho_K$ is regularly spaced.

This development is more general than Lucy's. Lucy's algorithm (Lucy 1974) algorithm was expressed for cases with $\int_{m_{\min}}^{m_{\max}} P(m|\rho) = 1$, which is not true in the case discussed here because the range of magnitudes is limited. The need for the denominator in eq. (13) was already recognized by Scoville et al. (1983).

The iteration converges when $N^r = N^{\text{obs}}$, i.e. when $\Delta^{r+1} = \Delta^r$. The first iterations produce a result which is close to the final answer, with the subsequent iterations giving only small corrections.

This algorithm has a number of good properties (Lucy 1974, 1994): both the luminosity function and the density are defined as being positive, the likelihood increases with the number of iterations, the method is insensitive to high frequency noise in N^{obs} , etc.

4.1 Stopping criteria for the iterative process and initial trial solution

From Lucy (1994), the appropriate moment at which to stop this kind of iterative process is when the curvature of the trajectory in the H-S diagram is a minimum. H and entropy (S) are defined by:

$$H = \sum_j N_j^{\text{obs}} \ln N_j^r \quad (15)$$

and

$$S = - \sum_i \Delta_i^r \ln \frac{\Delta_i^r}{\Delta_i^0}, \quad (16)$$

respectively, and the curvature in the H-S diagram is:

$$\kappa = \frac{|S' H'' - H' S''|}{(S'^2 + H'^2)^{3/2}}, \quad (17)$$

where the derivatives are with respect to the number of iterations, and the sums over i and j correspond to discrete values of the ρ and m integrals respectively.

Tests were carried out on the data set using this criterion (see an example in Fig. 4). In general there is a minimum after three iterations, corresponding to a non-relaxed state of the process. Afterwards, κ is increase up to around 10 iterations, where it then falls off again to a minimum, and then increases again. Apart from first minimum at 3 iterations, the most relevant minimum seems to be that at around 10 iterations.

However, this criterion is not very accurate for the noisiest cases and on occasions the last iteration may not be the most appropriate one to end at. Occasionally, it stops too early and therefore hinders the extraction of further information that could be exploited.

Therefore, the following criteria are adopted for ending the iterations:

- (i) The number of iterations must be greater than 10 and smaller than 10000. The process will always be stopped when the number of iterations exceeds 10000. The Δ^r variations are too small after 10000 iterations, so no more are made.
- (ii) For fewer than 1000 iterations, the iterative process is stopped when the solution is within the noise, i.e. when the average over m of the distance between $N^r(m)$ and $N^{\text{obs}}(m)$

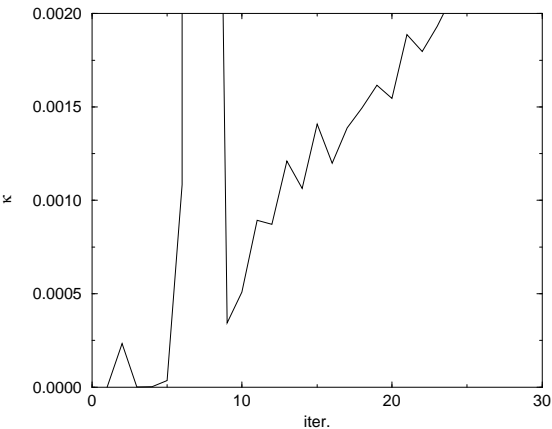


Figure 4. Curvature versus iteration number in an inversion case.

is less than the average over m of a random noise with Gaussian distribution of $N^{\text{obs}}(m)$ with $\sigma_m = S(N^{\text{obs}}(m))$, the Poissonian noise of $N^{\text{obs}}(m)$.

This last point will be clarified and the numerical algorithm to be used explained in what follows. N_i^r (the subindex i stands for the discrete value of m) is at s_i σ s from N_i^{obs} , i.e.

$$s_i = \frac{|N_i^r - N_i^{\text{obs}}|}{S(N_i^{\text{obs}})}. \quad (18)$$

The normalized probability of a point at distance s_i σ s from its real value is

$$p_i(s_i) = \text{erf}(s_i), \quad (19)$$

where $\text{erf}(x) = (2/\sqrt{\pi}) \int_0^x e^{-u^2} du$ is the error function. Thus, since the p_i distribution is nearly uniform between 0 and 1, then the s_i distribution follows

$$\frac{\sum_{i=1}^n p_i(s_i)^2}{n} \approx \int_0^1 p_i^2 dp_i = \frac{1}{3}. \quad (20)$$

'Nearly' because it is exact when $n \rightarrow \infty$, and there are some fluctuations when n is not too large.

Thus, within the noise means that

$$\frac{\sum_{i=1}^n p_i(s_i)^2}{n} < \frac{1}{3}, \quad (21)$$

and this is second stopping criterion.

The sum of p_i^2 is calculated instead of the sum of p_i because the difference distribution is not exactly Gaussian and a power of p_i gives a higher weighting to the large deviations (larger than 1-2 σ). In any case, this is only an approximate criterion.

The final solution does not depend on the initial trial solution, N^1 , when the number iterations is high enough. However, N^r may approach N^{obs} in a different way depending on the initial trial solution when the noise of the counts is high, because the process is stopped after a few iterations

which will give slightly different solutions. In order to avoid this influence for the noisiest data to be inverted[¶], the trial solution was fed back with the smoothed result of the previous inversion and inverted again. As will be discussed in §4.4, three inversions are made. In the second and the third iterations the trial solutions are fed back with the previous outcome, once it has been fitted to a smooth analytical function (in this case ellipsoids, as seen in §6).

4.2 Distance range

As the case described here is the application of the method to the bulge of our Galaxy, the numerical calculation of the distance integral are carried out over $2000 \text{ pc} < \rho_K < 30000 \text{ pc}$, as all of the stars are known to be contained within this distance. The real distance, r , is somewhat lower than ρ (see eq. 3), but the difference is small for low-extinction regions such as those used here.

It noted that, following numerical experiments with Lucy's algorithm, the minimum distance has to be kept within tolerable limits. Spurious fluctuations arise when small distances are included. This is related to the proportionality of the kernel to ρ^2 , so that large variations in the density at small distances do not significantly change the number of counts.

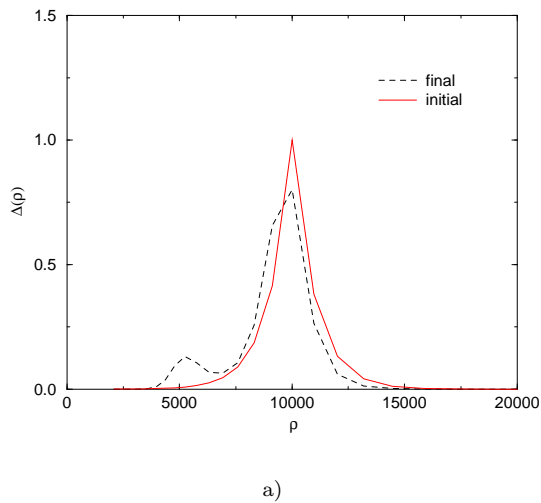
A similar problem arise for the maximum distance to which the sources can be distributed. If the maximum limit is too large then a spuriously high density might appear at large distances. The reason is that very distant stars should be very luminous to be observed and, since the luminosity function for very luminous stars is very small, any sources placed at a large distance will lead to a high density at that distance.

The application of this method to the bulge does not lead to problems since the distance range is known to be limited: the Galaxy has a boundary and the number of bulge stars in the solar neighbourhood is negligible. Nevertheless, it should be noted that care should be taken before applying this method to other Galactic components. For instance, it is possible that inverting the counts to obtain the Galactic disc density could encounter the above problems.

4.3 Example of application

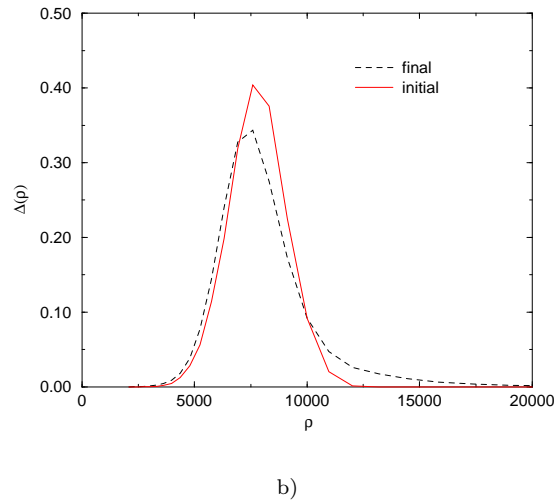
Inversion of the stellar statistics equation has been discussed by many authors, much more often in theory than in practice, and doubt has been cast on the viability of such an inversion. It has even even said that as the solution is non-unique (Gilmore 1989), which would lead to instability in the inversion. Except for some particular kernel functions (Craig & Brown 1986; ch. 4) this is not in fact the case, as we shall attempt to demonstrate here. The question of uniqueness is important only from a theoretical standpoint. In practice, the only relevant issue is whether the method is able to obtain a solution close to the real one when the counts are affected by noise, which always produces deviations from the real solution. The important thing is that

[¶] Very noisy data are eliminated. In this case, the 37 least noisy regions out of 71 are used when the density is the unknown function.



a)

Figure 5. Recovery of the theoretical luminosity function through the inversion process. Three cases: a), b), c).

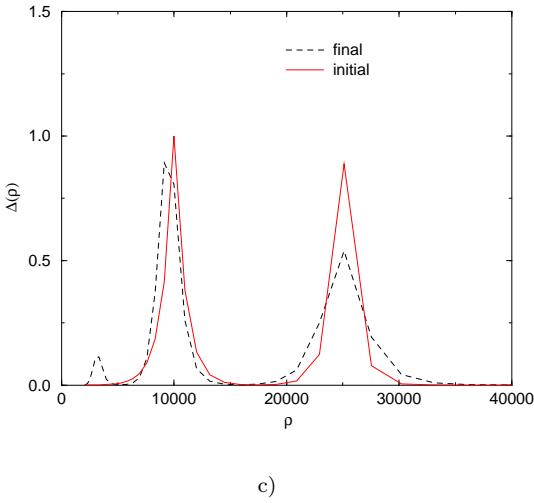


b)

this solution be not very far from the true solution. That the solution is not unique need not be important when all solutions be close to each other.

In order to test the reliability of the method, a number of simulations were made. A luminosity function and a fictitious density function were constructed. The cumulative count per square degree, $N(m)$, were then calculated by integrating eq. (6). A random noise with a Gaussian distribution is added to each bin. The cumulative counts with noise are then represented by $N^{\text{obs}}(m)$. When Lucy's algorithm is applied, with the same luminosity function and $\Delta^1(\rho) = 1$ (the choice of the trial initial solution does not affect the outcome), the results shown in Fig. 5 are obtained.

The inversion is not perfect since it is affected by the noise, but the results are fairly good. There is a “hump” in the first case at short distances, and a large increase in the density at large distances in the second case. However, it should be noted that the hump is at the 10% level of



the primary peak, which is located very close to the correct distance of 10000 pc. Similarly, the excess at large distances is at the level of only a few percent of the peak sources. Sensitivity to noise is higher for distances less than 7000 pc or greater than 15000 pc, as explained in §4.2, and this is reproduced in the experiments.

When the method is asked to recover two peaks, the inversion gives poorer results. However, were the number of iterations increased beyond the 10000 limit, then the second peak in Fig. 5 c) would rise and become closer to the original. Again, however, both peaks are correctly located and the total number of sources in each peaks is very close to the original. Apart from these details, the general shape of the peaks is recovered. Other numerical experiments were performed with similar results.

The bulge is a single-peaked structure so the proposed stopping criteria are sufficient. Since noise is random, the composition of the three-dimensional densities from the inversion for different regions (l, b) will attenuate the average deviations.

Application to equation (7), instead of (6), deserves similar considerations.

4.4 Method of deriving both the luminosity function and the density

The equations (6) and (7) can be solved for either the luminosity function or the density function, but not for both simultaneously for each region. Since both functions, Δ and Φ , are of interest but accurate information is not available for either of them, the following method was used.

To begin with, a first order approximation for the density was assumed. It was taken from the axisymmetric W92 model. A simple comparison showed that the W92 luminosity functions suggested that there were possible problems with the brightest sources, although the density function did give a reasonable starting point. Therefore, it was decided to solve first for the average luminosity function using the W92 bulge density.

With this density distribution, eq. (7) is inverted by means of Lucy's algorithm to provide the luminosity func-

tion for each of the regions (l, b) in Table 2. The weighted average of all luminosity functions was then calculated.

We have made the assumption that the bulge luminosity function is independent of position. This assumption is suspect (see Frogel 1988, Section 3) since the observed metallicity gradient might affect the luminosity of the AGB stars, although not the non-variable M-giants whose bolometric luminosity function is nearly independent of the latitude (Frogel et al. 1990). Some authors claim that there is a population gradient (Frogel 1990; Houdashelt 1996; Frogel et al. 1999), while others do not (Tyson & Rich, 1993, show that there is no metallicity gradient up to 10° out of the plane; Ibata & Gilmore, 1995, argue that there is no detectable abundance gradient in the Galactic bulge over the galactocentric range from 500 to 3500 pc). While the assumption may not be strictly true, it is nevertheless a useful approximation in deriving mean properties of the bulge.

With this averaged luminosity function, eq. (5) was inverted to derive a new density distribution by means of Lucy's algorithm for each region. In this step the 37 regions with the highest counts were used, as the determination of the density is more sensitive to noise.

The inversion of the luminosity function is more stable because the density distribution is sharply peaked and so the kernel in eq. (7) behaves almost as a Dirac delta function. Hence, the shape of the density distribution does not significantly affect the shape of the luminosity function.

The new density was then used to improve the luminosity function, etc. The whole process was iterated three times, which was enough for the results to stabilize as can be seen in Fig. 6: it is seen how the result of the third iteration is very close to the first, i.e. stabilization is reached in the first iterations. This small variation in successive iterations is really a convergence to the solution since, as is shown in §6.3.4 and §6.4.1, the counts are approximately recovered when we project the bulge obtained from the inversion.

The functions of interest are ϕ , the derivative of Φ , and D , related to Δ by the change of variable expressed in eqs. (3) and (4).

5 THE TOP END OF THE K LUMINOSITY FUNCTION

After three iterations the luminosity function was nearly independent of the position $(l, b)_i$, stable and hardly changed from the solution of the second iteration. Compare the first three iterations in Figure 6. In fact, even the first iteration came close to the final solution.

The obtained luminosity function is shown in Fig. 7 and in table 3. The derivative, ϕ , of $\Phi(M_K)$, from eqs. (7) and (2) is the normalized probability of having absolute magnitude M_K per unit absolute magnitude.

Figure 7 shows that for $-10 \text{ mag} < M_K < -8 \text{ mag}$ the bulge luminosity function is significantly lower than that of the disc (Eaton et al. 1984). Hence, the density of very bright stars in the bulge is much less than in the disc. Fainter than $M_K = -8 \text{ mag}$ the luminosity functions of the disc and the bulge coincide, in agreement with Gould (1997). The luminosity function for $-10 \text{ mag} < M_K < -8 \text{ mag}$ is significantly below the synthesized luminosity function assumed by W92 for the bulge in their model of the Galaxy (this can also be

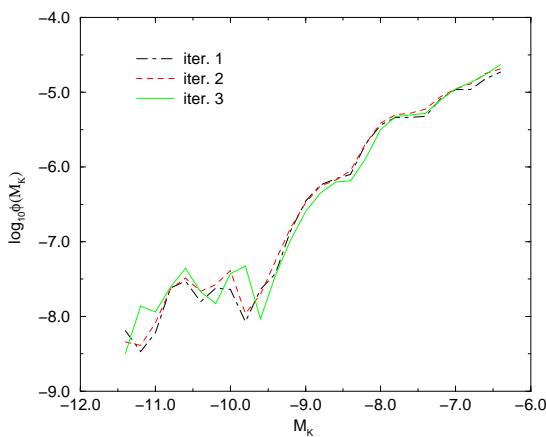


Figure 6. Luminosity function in the first three iterations.

clearly seen in the W92 model and the TMGS in Hammerley et al (1999)). This discrepancy could arise from their not having taken into account that the brightest stars in the bulge are up to 2 mag fainter than the disc giants (Frogel & Whitford 1987). This would shift the W92 luminosity function to the right in Figure 7. It should be remembered that the W92 model was developed to predict the *IRAS* source counts. *IRAS* could see only the very top end of the bulge luminosity function, and the sources responsible are all dust-shrouded AGB stars. The dust enormously brightens the 12 and 25 micron fluxes over the expected photospheric flux. In fact, at the distance of the bulge, *IRAS* could not see purely photospheric stars at all. The TMGS, however, can detect normal bulge M giants (Frogel & Whitford 1987), not only AGBs, and the presence of dust leads only to a minor increase in the K brightness. Therefore, in the TMGS while it is true that we do see the extreme AGB stars detected by *IRAS*, they in fact represent only a tiny fraction of the detected sources in each magnitude bin. Hence, the top end of the *IRAS* luminosity function and the top end of the TMGS luminosity function are dominated by different types of sources and so W92 could be close for *IRAS* but not get the top end of the K star counts correct.

Between $M_K = -8$ mag and $M_K = -6$ mag (corresponding to the fainter limit of the TMGS at the distance of the bulge) the luminosity function of W92 does coincide with that determined here. As has already been noted, the result from the first iteration of the luminosity function (when the assumed density function was that of W92) is very close to the final result, particularly for absolute magnitudes fainter than $M_K < -8$ mag. This implies that for the lines of sight used here the W92 model does correctly predict the number of bulge stars per magnitude per square degree for $-8 \text{ mag} < M_K < -6 \text{ mag}$, even though this model was aimed at matching the *IRAS* source counts. Given the match over this magnitude range we have chosen to use the W92 luminosity function for the magnitudes fainter than $M_K = -6$ mag, so that the luminosity function can be normalized.

Comparison with the bolometric luminosity function obtained by other authors (see references in the introduc-

Table 3. K -band luminosity function for bulge stars.

M_K (mag)	$\log_{10} \phi$	M_K (mag)	$\log_{10} \phi$
-11.4	-8.50 ± 0.50	-8.8	-6.35 ± 0.33
-11.2	-7.87 ± 0.48	-8.6	-6.20 ± 0.31
-11.0	-7.94 ± 0.43	-8.4	-6.19 ± 0.28
-10.8	-7.61 ± 0.43	-8.2	-5.88 ± 0.30
-10.6	-7.36 ± 0.44	-8.0	-5.50 ± 0.20
-10.4	-7.67 ± 0.66	-7.8	-5.32 ± 0.17
-10.2	-7.83 ± 0.83	-7.6	-5.30 ± 0.22
-10.0	-7.43 ± 0.68	-7.4	-5.28 ± 0.23
-9.8	-7.33 ± 0.79	-7.2	-5.10 ± 0.17
-9.6	-8.03 ± 1.22	-7.0	-4.96 ± 0.12
-9.4	-7.45 ± 0.85	-6.8	-4.87 ± 0.19
-9.2	-6.98 ± 0.58	-6.6	-4.76 ± 0.10
-9.0	-6.60 ± 0.46	-6.4	-4.63 ± 0.14

tion) is not possible since bolometric corrections are not available. Also, in most of cases the magnitude interval is different. Tiede et al. (1995) provide, by combining data from different works, the luminosity function in the K band as a function of the apparent magnitude in the range 5.5 mag $< M_K < 16.5$ mag. The brightest magnitudes are taken from Frogel & Whitford (1987). The comparison with our luminosity function is not direct since they have not normalized their luminosity function to unity; moreover, they have not taken into account the narrow but non-negligible dispersion of distances. In Fig. 16 of Tiede et al. (1995) there is a fall-off in the luminosity function for $M_K \leq 6.5$ mag or in Fig. 18 of Frogel & Whitford (1987) for $M_{\text{bol}} \leq -4.2$ mag, which could be comparable with that of our luminosity function at $M_K \approx -8.0$ mag. However, because of the much larger area covered by the TMGS, the error for the brightest magnitudes is far lower in this paper, the result being pushed well above the noise; this is not the case for Frogel & Whitford (1987).

The presented luminosity function for very bright stars (brighter than $M_K \sim -9.5$ mag) is of low precision. The number of bulge stars in this range is very small, so even small errors due to contamination from the spiral arms will mean that the luminosity function is overestimated and so the values should be taken as an upper limit.

5.1 Age of the bulge

The age of the bulge is an open topic. There are authors who think the bulge is older than the halo (Lee 1992) whilst others hold the opposite opinion (Rich 1993). Although from the work presented here an accurate value for its age cannot be determined, the bulge is clearly older than the disc. The lack of very luminous stars in the bulge means that there are few supergiants and bright giants, and hence star formation regions. A comparison between the K -band luminosity function derived here and models of stellar evolution could provide some further clue in this controversial subject. The model of Bertelli et al. (1994), with a 10-Gyr population and solar metallicity, predicts that all the stars should be fainter than $M_K = -8$ mag, while these data show that there are some sources of -9.5 and -8 mag. This may indi-

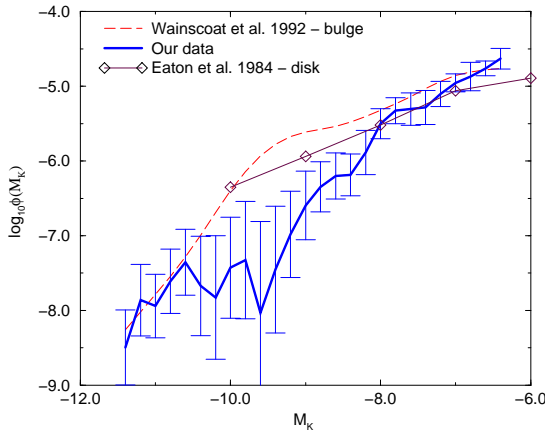


Figure 7. Luminosity function in the K -band (solid line). Comparisons with W92 in the bulge and Eaton et al. (1984) in the disc are also provided.

cate a mixture of populations with different ages embedded in the bulge.

6 DENSITY DISTRIBUTION

6.1 Density along the line of sight

The second result is the density $D(r)$ for each region (l, b) , i.e. some points of the function $D(\vec{r}) = D(r, l, b)$. Δ is obtained by inversion of eq. (6) and then changing the variable in eq. (3) to recover $D(r)$.

As an example, the density distribution along the line of sight for one region ($l = 5.4^\circ$, $b = 3.7^\circ$) is shown in Fig. 8 after extinction correction. As can be seen, the bulge distribution of stars has a maximum around 8 kpc. There is a rise from ~ 5 kpc to ~ 8 kpc, and a fall off after this. Similar results were obtained in the other regions, except for some fluctuations due to errors (the errors in the counts may provide this fluctuation; see §4). The 37 regions used were the least noisy and least affected by patchy extinction.

6.2 Bulge cuts

As was said in §2, the regions come from strips with constant declination: $\delta = -30^\circ$, $\delta = -22^\circ$ and $\delta = -16^\circ$. The 37 regions used for density inversion are come from the strips at $\delta = -30^\circ$, $\delta = -22^\circ$ (as the bulge source density by $\delta = -16^\circ$ is low). A strip can be thought of as a surface in space (Fig. 9) one axis is in R.A. (i.e. constant declination) and the other is distance along the line of sight, which can be converted to a distance parallel to the Sun–Galactic center line. Figures 10 and 11 show these plots with the z -axis representing the density. Note that the density scale (height) is different in both figures.

As can be seen, there are two peaks and a valley in both figures. The valley only indicates the absence of data due to the fact that the Galactic plane between $b = -2^\circ$ and $b = 2^\circ$

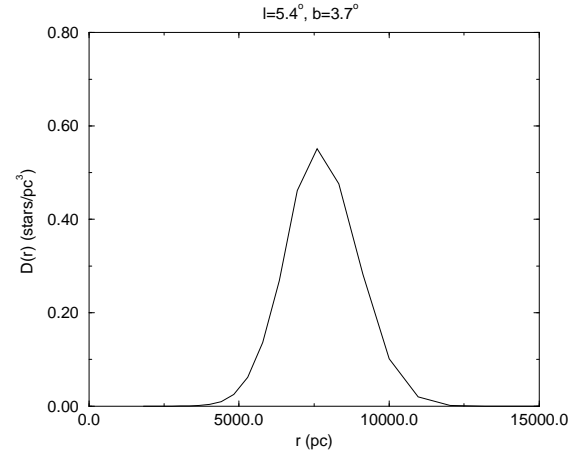


Figure 8. Density along the line of sight in the region ($l = 5.4^\circ$, $b = 3.7^\circ$).

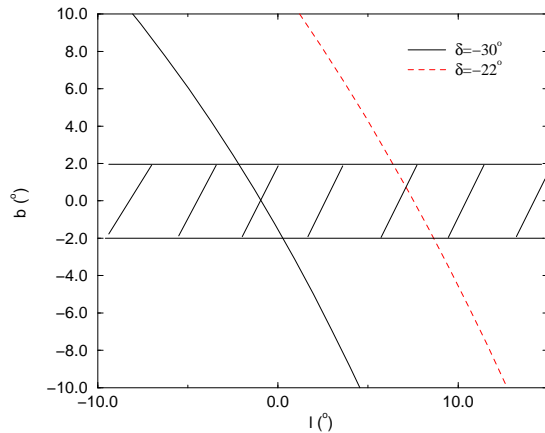


Figure 9. Two constant-declination strips that cut the disc. The striped region is the Galactic plane zone, which was excluded.

was avoided. If the plane data were included there would be only one peak.

Galactic longitude increases and latitude decreases with increasing x . In Fig. 11, the left side (negative x) of the valley has a lower density than the right side (positive x) due to the abrupt fall-off of the density with distance from the Galactic center. This is not observed in Fig. 10 because this strip almost cuts across the Galactic center so both sides of the valley are nearly symmetric.

When comparing the position of the peaks, and hence the maximum density, in both figures, the peaks are noticeably closer to the Sun for $\delta = -22^\circ$ ($l = 7.5^\circ$) than for $\delta = -30^\circ$ ($l = -1^\circ$). The non-axisymmetry of the bulge is the most plausible explanation for this and the bulge is closer to us at higher galactic longitudes. This can, in fact, be seen in the individual strips, as the left peak (i.e. larger l) is closer than the right one in both figures. Hammersley et

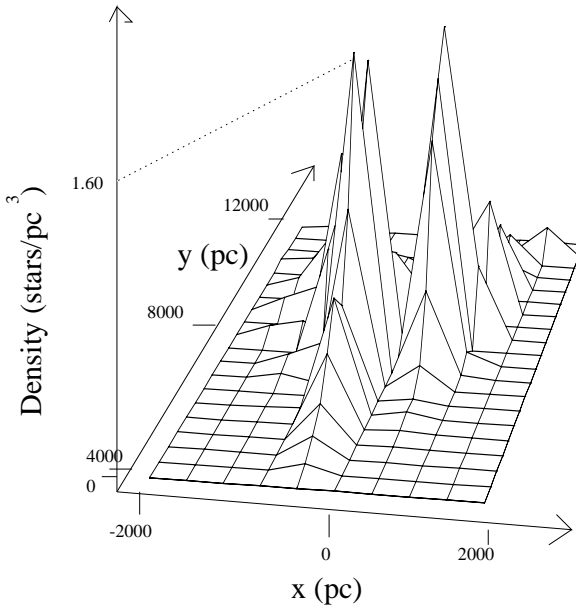


Figure 10. Plot of the density (height) as a function of both spatial coordinates defined by a cut of the bulge in $\delta = -30^\circ$. Galactic latitude is increased from left to right (x -axis). The y -axis is distance parallel to the line joining the Sun to the Galactic Centre. The grid scale is 400 pc for each small square. The range of distances is from 4000 to 12000 pc along the line of sight, and from -2000 to $+2000$ pc in the x -axis. The origin is at the Sun.

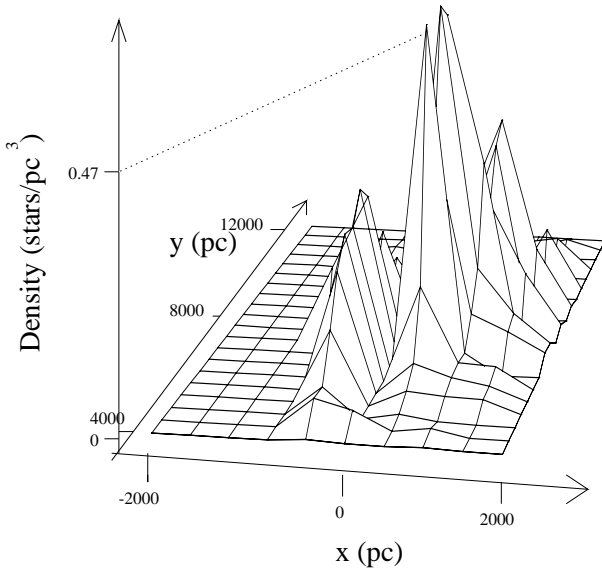


Figure 11. The same plot as Figure 10 but for $\delta = -22^\circ$.

al. (1999: Sect. 7, Fig. B) also show this asymmetry derived from TMGS data.

6.3 The three-dimensional bulge

The morphology of the bulge can be examined by fitting the isodensity surfaces to $D(\vec{r}) = D(r, l, b)$. The results of

the previous subsection argued for non-axisymmetry in the bulge, so the next stage was to determine the parameters.

Ellipsoids were used for the fit, with two axes in the Galactic plane and a third perpendicular to these. The possible tilt of the bulge out of the plane was neglected as there is no evidence for this (Weiland et al. 1994). Also the position of the Sun 15 pc above the plane (Hammersley et al. 1995) does not have a significant influence since the bulge extends much further from the plane.

The Galactocentric distance along the major axis for different isodensity ellipsoids is

$$t = \sqrt{x_1^2 + K_2^2 x_2^2 + K_z^2 z^2} \quad (22)$$

and the distance along the minor axis is t/K_z . The projections of the vector distance to the Galactic centre are represented x_1 and x_2 (Fig. 12), and z is the distance to the plane. K_2 and K_z are the axial ratios between axes x_1 and x_2 , and x_1 and z , respectively. Both ratio are defined to be greater than one.

From the same figure x_1 and x_2 are defined as follows:

$$x_1 = R \cos(\beta - \alpha) \quad (23)$$

and

$$x_2 = R \sin(\beta - \alpha), \quad (24)$$

with

$$R = \sqrt{(r \cos b)^2 + R_0^2 - 2rR_0 \cos b \cos l}, \quad (25)$$

$$z = r \sin b, \quad (26)$$

and, following the sine rule,

$$\beta = \sin^{-1} \frac{r \cos b \sin l}{R}. \quad (27)$$

The ellipsoids have four free parameters: R_0 , the Sun-Galactic centre distance (the ellipsoids are then centred on this position); K_z and K_y , the axial ratios with respect to the major axis (x); and α , the angle between the major axis of the triaxial bulge and the line of sight to the Galactic centre (α between 0° and 90° is where the tip of the major axis lies in the first quadrant).

Three-dimensional ellipsoids are fitted to 20 isodensity surfaces (from 0.1 to 2.0 star pc $^{-3}$, in steps of 0.1) with the four free parameters.

The four parameters are then averaged for the 20 ellipsoids and the results are:

$$R_0 = 7860 \pm 90 \text{ pc},$$

$$K_2 = 1.87 \pm 0.18,$$

$$K_z = 3.0 \pm 0.9$$

and

$$\alpha = 12 \pm 6 \text{ deg}. \quad (28)$$

The errors are calculated from the average of the ellipsoids and so do not include possible systematic errors (for example: subtraction of the disc, contamination from other components, methodological inaccuracies of the inversion, etc.), which are difficult to determine. However, by far the largest effect on the bulge counts is the massive asymmetry in the counts caused by the triaxiality of the bulge, as

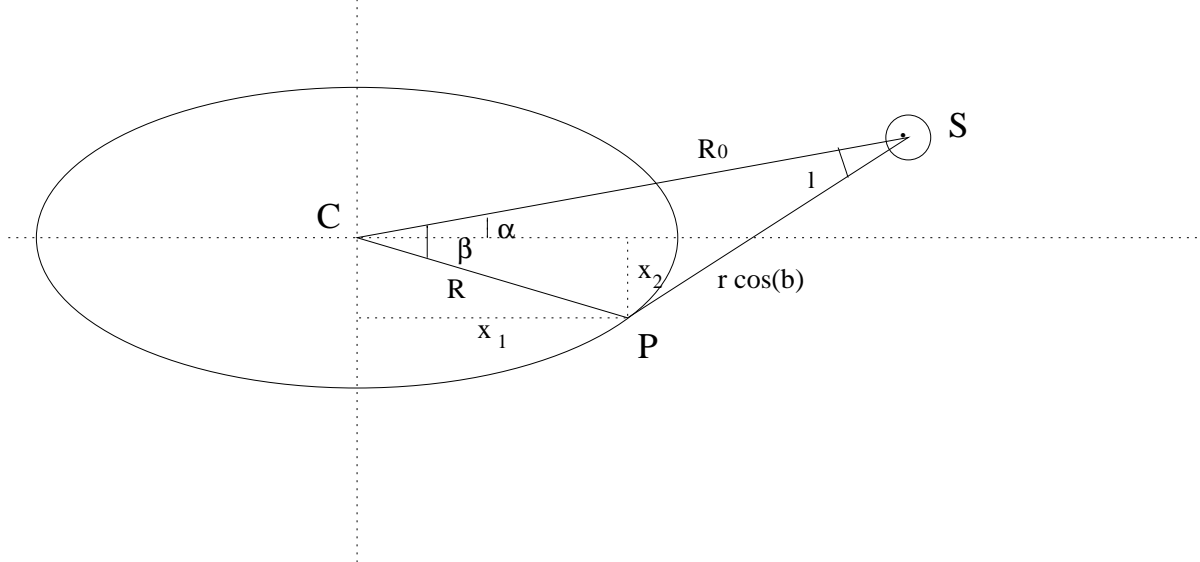


Figure 12. Cut of an ellipsoidal bulge in the Galactic plane. C is the Galactic centre, P is a given point on the ellipsoid and S is the Sun.

shown in Hammersley et al. (1999). The other systematic effects are at least an order of magnitude below this, so while they do have an effect, it is small. Hence, the true errors are larger than stated but tests suggest that they do not alter the general findings presented here.

The error in K_z is quite large and is due to the non-constant axial ratio of the ellipsoids. K_z tends to increase towards the centre, i.e. the outer bulge is more circular than the inner bulge. This will be further discussed in §6.4.

6.3.1 Axial ratios and orientation

The axial ratios of the bulge are 1:0.54:0.33. These numbers indicate that the bulge is triaxial with the major axis close to the line of sight towards the Galactic centre. In general, the result presented here are in agreement with those from other authors. The projection, as viewed from the position of the Sun, of an ellipsoid of the above characteristics, gives an ellipse with axial ratio 1.7 ± 0.5 (i.e. 1:0.58). This is compatible with the value of 1:0.6 obtained by Weiland et al. (1994) or 1:0.61 by (Kent et al. 1991).

From a dynamic model assuming a gas ring in a steady state, Vietri (1986) finds axial ratios of 1:0.7:0.4, which is close to our result. Binney et al. (1991) found $\alpha = 16$ deg for a bar, i.e. a triaxial structure in the centre of the Galaxy, in order to explain the kinematics of the gas in the centre of the Galaxy. Weinberg (1992) gives $\alpha = 36 \pm 10$ deg and $K_2 = 1.67$ from his analysis of *IRAS* data. More recently, Nikolaev & Weinberg (1997) obtained a bar from *IRAS* sources with $\alpha = 19$ deg and K_2 between 2.2 and 2.7. Stanek et al. (1997), based on the analysis of optical photometric data for regions of low extinction, predicted an α between 20 and 30 deg and 1:0.43:0.29 axial ratios, which is also quite close to the result presented here. Various authors have examined the *COBE-DIRBE* flux maps for triaxiality: Dwek et al. (1995) give higher eccentricity values for the axial ratios, 1:0.33:0.22,

but the angle $\alpha = 20 \pm 10$ deg is compatible with the value given here; Binney et al. (1997) derive 1:0.6:0.4 ratios and an angle $\alpha \sim 20$ deg; Freudenreich (1998) obtained a best fit with 1:0.38:0.26 ratios and $\alpha = 14$ deg. Normally, when the low latitudes are excluded the fit of the triaxial bulge has an angle of about 25 degrees (Sevenster et al. 1999). The majority of the above authors did not use inversion; rather they fitted the flux or the star counts to models using a priori assumptions. Binney et al. (1997) were the exception in using inversion on the *COBE-DIRBE* surface-brightness maps^{||} and, on the basis of specific assumption, obtained results close to those presented here.

6.3.2 Galactocentric distance

The distance R_0 derived here is slightly less than that used in the W92 model of the disc (8.5 kpc). However, the small changes in R_0 can be compensated by small changes in the other model parameters, such as the scale length, so that the predicted counts remain the same. As the model used already gave a good fit to the disc, we decided not to make ad hoc modifications to account for a smaller R_0 since the disc is not the subject in this paper.

The lack of previous assumptions makes the determination of R_0 presented here different from those of other authors. In particular, no information is required on the objects observed. However, the values determined here are very close to the currently accepted value of just under 8 kpc. Reid et al. (1988) deduce a value $R_0 = 7.1 \pm 1.5$ kpc from

^{||} The inversion of the flux and the inversion of the star counts are significantly different. Since star counts provide a function for each region of space and the flux is only one number for each of those regions, the inversion of the flux is less suitable for directly extracting information from the data and further assumptions are needed.

Table 4. Relationship between the maximum distance of the ellipsoid and the bulge star density.

t (pc)	D (pc $^{-3}$)	t (pc)	D (pc $^{-3}$)
3020 ± 810	0.1	1620 ± 250	1.1
2630 ± 650	0.2	1580 ± 240	1.2
2420 ± 590	0.3	1540 ± 240	1.3
2230 ± 490	0.4	1460 ± 230	1.4
2120 ± 450	0.5	1420 ± 230	1.5
1990 ± 380	0.6	1390 ± 230	1.6
1900 ± 350	0.7	1380 ± 240	1.7
1840 ± 330	0.8	1360 ± 250	1.8
1720 ± 280	0.9	1360 ± 260	1.9
1670 ± 270	1.0	1320 ± 220	2.0

direct observations of Sgr B2. Gwinn et al. (1992), by means of observations of masers in W49, derive $R_0 = 8.1 \pm 1.1$ kpc. Moran (1993) obtains $R_0 = 7.7$ kpc, from OH/IR stars distances. Turbide & Moffat (1993) obtain $R_0 = 7.9 \pm 1.0$ kpc, from measurements of the distances to young stars by means of CCD photometry and assuming that there is no metallicity gradient in the outer regions of the Galaxy; although they get 7.2 kpc when a certain gradient is assumed. Paczyński & Stanek (1998) derived $R_0 = 7.97 \pm 0.08$ (systematic effects make the true error larger) from the comparison between *Hipparcos* and OGLE data. Olling & Merrifield (1998a, 1998b) obtain $R_0 = 7.1 \pm 0.4$. Etc. Generally, many studies based on indirect measurements claim the Galactocentric distance to be somewhat less than 8.0 kpc (see also the review by Reid, 1993).

6.3.3 Density as a function of the distance to the Galactic centre

A power law with exponent -1.8 is observed in the centre of the bulge and also in other galaxies (Becklin & Neugebauer 1968; Sanders & Lowinger 1972; Maihara et al. 1978; Bailey 1980; see review by Sellwood & Sanders 1988). When the density function $D(t)$ (Table 4) is fitted to $D(t) = A(t/t_0)^{1.8} \exp(-(t/t_0)^\gamma)$, with γ , t_0 and A as free parameters, then we obtain

$$D(t) = 1.17(t/2180 \text{ pc})^{-1.8} \exp(-(t/2180 \text{ pc})^{1.8}) \text{ star pc}^{-3}. \quad (29)$$

This gives an estimate of the fall-off in density between 1.3 and 3.0 kpc from the centre in the direction parallel to the major axis or between 0.4 and 1.0 kpc in the direction perpendicular to the plane. As can be seen in Fig. 13, the dispersion of points around this law is large, so it is possible to accommodate other functions or even a different set of parameter. A different luminosity function amplitude would change the amplitude of the stellar density, A . If the normalization for the luminosity function were incorrect then the factor needed to multiply the luminosity function would be used to divide the star-density amplitude.

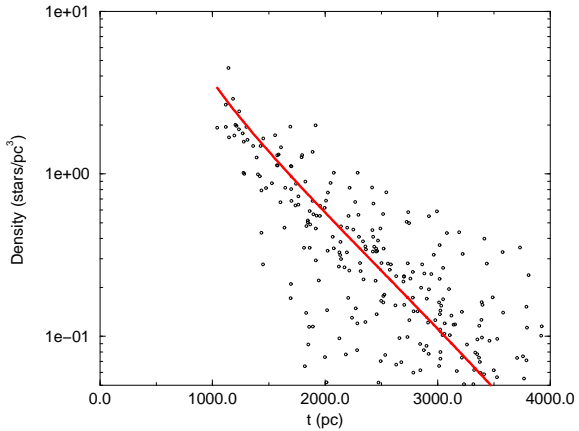


Figure 13. Fit of the density distribution. The solid line is the best fit using eq. (29).

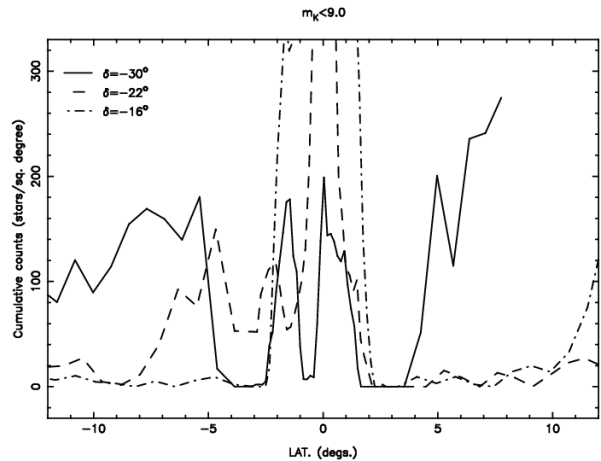


Figure 14. $N(m_K = 9.0 \text{ mag})$ along the three strips that are used with constant declinations: $\delta = -30^\circ$, which cuts the plane at $l = -1^\circ$; $\delta = -22^\circ$, which cuts the plane at $l = 7^\circ$; and $\delta = -16^\circ$, which cuts the plane at $l = 15^\circ$ once the W92 disc and bulge (according to eqs. (28) and (29)) are subtracted.

6.3.4 Goodness of the inversion

The residual counts for $m_K < 9$ after subtracting both the bulge determined here and the W92 disc model from the original counts are plotted in Figure 14. As can be seen, the off-plane residual counts (the $|b| < 2^\circ$ regions are clearly contaminated by other components) are reduced to typically a few per cent of the original counts shown in Figure 2. For the $\delta = -30^\circ$ strip the residuals are typically 100 star/deg 2 compared to the 1500 star/deg 2 in the original counts. Hence the proposed bulge parameters do accurately reproduce the observed counts.

6.3.5 A triaxial bulge

From Figs. 10 and 11, the non-axisymmetry was determined for the plane. Furthermore, the axial ratio K_2 is close to 2 (and not 1, the condition of axisymmetry). Therefore the bulge is a triaxial ellipsoid orientated in such a way that the minor axis is perpendicular to the Galactic plane, and the angle between the major axis and the Sun–Galactic centre line is 12° in the first quadrant.

Whether this structure is called a bar or triaxial bulge is not only a question of wording. Apart from the morphology, the population is also has to take into account: bulges are older than bars (Kuijken 1996), though both are older than the disc. Precise calculations of the age (see §5.1) would be necessary to differentiate between them. However, there is evidence of another lengthened structure, a bar, (Hammersley et al. 1994; Calbet et al. 1996; Garzón et al. 1997) whose angle is $\sim 75^\circ$ in the first quadrant. This has major star formation regions at both extremes (towards $l = 27^\circ$ and $l = -22^\circ$) and there is evidence for a preceding dust lane (Calbet et al. 1996). If this other component exists then the structure discussed in this paper must be called a “bulge”, unless we are prepared to entertain the notion that the Galaxy has two bars.

6.4 Bulge with variable K_z ellipsoids

A large error in K_z is obtained when it is assumed constant, as was indicated in the previous subsection. Therefore, it is possible that the K_z values are not constant, and so another dependence on the isodensity contours was tried. When the ellipsoids are fitted allowing a linearly variable K_z , then

$$K_z = (1.66 \pm 0.17) + (1.73 \pm 0.14)D \quad (30)$$

(where the units of D are star pc^{-3}), whose weighted average is $K_z = 3.0$, as obtained in eq. (28). The other parameters (K_2 , R_0 and α) remain nearly constant with respect to D .

This variation of K_z is independent of the trial solution in the iteration process (see §4.1). A fourth iteration was performed for both the luminosity function and the density with the feed-back of the variable K_z , and it could be seen that the same parameters are recovered again, within a 1σ error. Indeed, the x_1-z ratio is

$$K_z = (1.76 \pm 0.32) + (1.70 \pm 0.27)D. \quad (31)$$

This linear dependence is valid in the density interval from 0.1 to 2.0 star pc^{-3} . For highest densities, K_z is expected to grow more slowly. K_z can also be expressed as a function of t , although this dependence is non-linear. The fit to an exponential law is:

$$K_z = (8.4 \pm 1.7) \exp\left(\frac{-t}{(2000 \pm 920) \text{ pc}}\right) \quad (32)$$

and is valid for the range of distances, t , used here (see Fig. 16). Figure 15 shows the variation of eccentricity as a function of the density.

With K_z so defined, the density, D , is given by Table 5 or Figure 16.**.

** The density is expressed as a function of t/K_z , the distance along the z -axis, because the variation of K_z with t fluctuates too

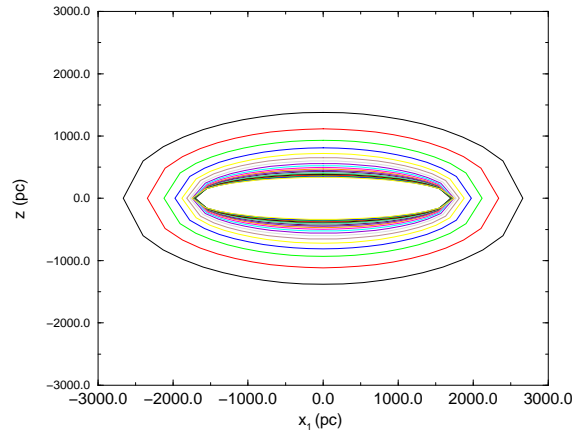


Figure 15. Cut of the bulge in the x_1-z plane when K_z is given by eq. (32). The ellipses represent isodensity lines between 0.1 and 2.0 star pc^{-3} , with intervals of 0.1.

Table 5. Relationship between the distance along the minor axis, t/K_z and the density, when K_z is given by (32).

t/K_z (pc)	D (star pc^{-3})	t/K_z (pc)	D (star pc^{-3})
1400 ± 380	0.1	470 ± 60	1.1
1170 ± 290	0.2	440 ± 50	1.2
1010 ± 240	0.3	430 ± 40	1.3
880 ± 200	0.4	410 ± 40	1.4
780 ± 160	0.5	390 ± 40	1.5
700 ± 140	0.6	380 ± 30	1.6
640 ± 120	0.7	370 ± 30	1.7
570 ± 100	0.8	360 ± 30	1.8
540 ± 90	0.9	350 ± 30	1.9
510 ± 80	1.0	330 ± 20	2.0

The best fit to a law of type $D(t/K_z) = A(t/(K_z t_0))^{-1.8} \exp(-(t/(K_z \times t_0))^\gamma)$ is:

$$D(t/K_z) = 0.106 \left(\frac{t/K_z}{1820 \text{ pc}} \right)^{-1.8} \exp \left(- \left(\frac{t/K_z}{1820 \text{ pc}} \right)^{5.4} \right) \text{star pc}^{-3}. \quad (33)$$

6.4.1 Goodness of the inversion

The residual counts after both the bulge determined here with variable K_z and the W92 disc model are subtracted from the original counts for $m_K < 9$ are plotted in Figure 17. As can be seen the residuals are now somewhat lower than when K_z is constant (Fig. 14). Typically the residuals are now 50 to 100 star/deg^2 and the maximum has fallen from 300 star/deg^2 with constant K_z to 200 star/deg^2 . Therefore,

much. The ellipsoid size decreases when the density, D , increases; however, K_z increases with D , so the axis x_1 increases. Hence, the variation of D as a function of t is too sensitive to noise.

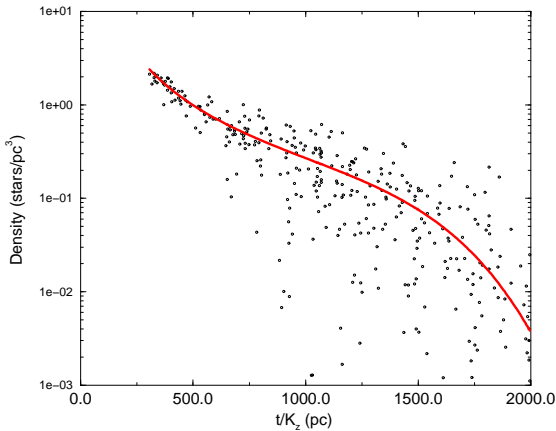


Figure 16. Fit of the density distribution when K_z is given by eq. (32). The solid line stands for the fit to (33).

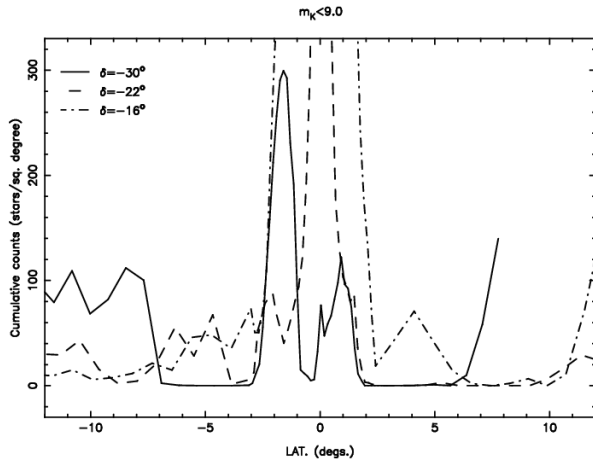


Figure 17. $N(m_K = 9.0 \text{ mag})$ along the three strips that are used with constant declinations: $\delta = -30^\circ$, which cuts the plane at $l = -1^\circ$; $\delta = -22^\circ$, which cuts the plane at $l = 7^\circ$; and $\delta = -16^\circ$, which cuts the plane at $l = 15^\circ$ once the W92 disc and bulge (according to eqs. (28), (32) and (33)) are subtracted.

the variable K_z does provide a better fit to the observed counts.

The aspect of the bulge as seen by an observer far away in the z -axis, i.e. the Galaxy observed face-on, would be as shown in Figure 18. The sharp fall-off in density is very noticeable. The bulge in a face-on Milky Way-like Galaxy presents, according to our results, a very high contrast between central regions (with up to $10000 \text{ star pc}^{-2}$) and regions at 3 kpc in the major axis (with 100 star pc^{-2}).

Whether this variation of K_z is a true feature of the density distribution or not is a matter for further investigation. However, this is observed in other galaxies (Varela et al. 1993) and we do not believe that the result of this subsection is due to systematic errors, although this possibility cannot be totally excluded.

Other possible causes for this might be either that a

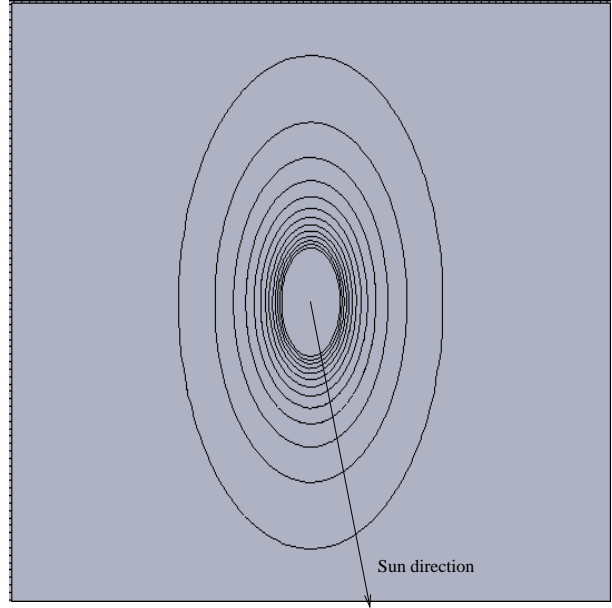


Figure 18. Projection of the bulge, eq. (32), when it is observed face-on (integration of z direction). The square is $8 \text{ kpc} \times 8 \text{ kpc}$ centred on the Galactic Centre. The outer contour represents 10 star pc^{-2} , the second contour stands for 410 star pc^{-2} , etc., and the inner contour stands for $4810 \text{ star pc}^{-2}$ (the interval between consecutive contours is 400 star pc^{-2}).

superposition of two components is being observed, i.e. the bulge and another structure, a bar, closer to the plane. If this were true, the luminosity function would have two different populations, especially in the regions closest to the plane. A gradient within the bulge is also possible. A greater number of bright stars in the innermost bulge (as observed by Calbet et al. 1995), with a smooth variation from the inner to the outer bulge, could be responsible of this effect. Both of these causes would lead to a gradient in the luminosity function. However, as the luminosity function has been assumed to be constant the result after inversion would be a gradient in K_z . Tests on the data indicate that this is possible. Giving the luminosity function a gradient in z , but such that the luminosity function remains within the error bars for a determined average function, is sufficient to produce changes in the observed gradient in K_z . In any case, the errors in the luminosity function (see Table 3) do limit this variation of populations.

6.5 Stellar content of the bulge

Integrating the density over all space will give the stellar content of the whole bulge:

$$N = \int D(t) dV. \quad (34)$$

The volume element dV , under a change of variable to elliptic coordinates t , θ and ϕ , is related to the Cartesian coordinates $x = t \sin \theta \cos \phi$, $y = \frac{t}{K_2} \sin \theta \sin \phi$, $z = \frac{t}{K_z} \cos \theta$, through

$$dV = h_t h_\theta h_\phi dt d\theta d\phi, \quad (35)$$

with

$$h_i = \sqrt{\left(\frac{\partial x}{\partial q_i}\right)^2 + \left(\frac{\partial y}{\partial q_i}\right)^2 + \left(\frac{\partial z}{\partial q_i}\right)^2}. \quad (36)$$

Hence,

$$\begin{aligned} dV = t^2 \sin \theta \sqrt{\sin^2 \phi + \frac{\cos^2 \phi}{K_2^2}} \\ \times \sqrt{\frac{\sin^2 \theta}{K_z^2} + \cos^2 \theta \left[\cos^2 \phi + \frac{\sin^2 \phi}{K_2^2} \right]} \\ \times \sqrt{\frac{\cos^2 \theta}{K_z^2} + \sin^2 \theta \left[\cos^2 \phi + \frac{\sin^2 \phi}{K_2^2} \right]} dt d\theta d\phi. \end{aligned} \quad (37)$$

The result is 2.8×10^{10} stars for $K_z = 3$ with D from eq. (29); and 4.1×10^{10} stars with a variable K_z from eq. (32) and D from eq. (33), i.e. a factor 1.4 greater. This is, of course, only an estimation which includes an extrapolation of D to all space and the assumption of a correct luminosity-function normalization (see §5). Nevertheless, it leads to an order of magnitude for the mass of the Galactic bulge (taking an average mass for a star of $\sim 1 M_\odot$) compatible with other data (for instance, $\sim 2 \times 10^{10} M_\odot$ in Gould 1997); so this supports the normalization and the extrapolation. From the integration of the luminosity function it is found that TMGS stars from the whole bulge ($m_K < 9.0$ mag) represent only a fraction ($\sim 2 \times 10^{-5}$) of the total number of stars, i.e. 6×10^5 stars for $K_z = 3$.

7 HOW DIFFERENT WOULD THE RESULTS FOR A DIFFERENT DISC MODEL BE?

Errors in different parts of the inversion procedure used here will lead to changes in the results. One important source of error may be the disc model that is used: were a different model to be used, the answers would be different. Clearly the answer to a certain extent depends on the new model to use. As has been detailed earlier in §3.3, the disc model used here is in good agreement with the observed TMGS star counts where the disc is isolated and so the expectation is that its extrapolation to regions where bulge and disc are observed will lead only to small errors in the counts. By definition, the bulge is an excess over the extrapolated disc in central regions of the Galaxy so, also by definition, the error of the present disc model cannot be very large once its fitting to observational data in external parts of the Galaxy has been tested.

From the integral equation (6), it can be deduced that these errors, $\delta N_{K,\text{disc}}(m_K)$, follow for all regions (l, b) :

$$\begin{aligned} \delta N_{K,\text{disc}}(m_K) = -\omega \\ \times \int_0^\infty \delta \Phi_{K,\text{bulge}}(m_K + 5 - 5 \log_{10} \rho_K) \Delta_{\text{bulge},K}(\rho_K) \rho_K^2 d\rho_K \\ - \omega \int_0^\infty \Phi_{K,\text{bulge}}(m_K + 5 - 5 \log_{10} \rho_K) \delta \Delta_{\text{bulge},K}(\rho_K) \\ \times \rho_K^2 d\rho_K, \end{aligned} \quad (38)$$

If we know $\delta N_{K,\text{disc}}(m_K)$, which differentiates the “real disc” from our model, we could derive how large $\delta\Phi$ and $\delta\Delta$ are. The inversion procedure explained in §4 produces solutions which are close when we begin the iteration from counts that are similar, as can be seen from eq. (13). Hence, for small $\delta N_{K,\text{disc}}(m_K)$, $\delta\Phi$ and $\delta\Delta$ are also small. That is, the behaviour is not a chaotic such that small departures from the original counts would not produce very different solutions.

For instance, let us suppose that there is an error, δh_R , in the scale length of the disc (equal to 3.5 kpc in the W92 model we assumed). This leads to an error in the density due to the disc of

$$\delta D_{\text{disc}} = D_{\text{disc}} \frac{\delta h_R (R - R_\odot)}{h_R^2}, \quad (39)$$

where R is distance from the Galactic centre and R_\odot is this distance for the Sun (8.5 kpc in the W92 model). Hence, by means of eqs. (3), (4) and (5) for the disc,

$$\begin{aligned} \delta N_{K,\text{disc}}(m_K) = \omega \frac{\delta h_R}{h_R^2} \int_0^\infty \Phi_{K,\text{disc}}(m_K + 5 - 5 \log_{10} \rho_K) \\ \times \Delta_{\text{disc},K}(\rho_K) (R - R_\odot) \rho_K^2 d\rho_K, \end{aligned} \quad (40)$$

which can be set equal to expression (38) for all m_K , l and b . However, whilst in principle the change in the disc is proportional to the scale length, and there are certainly values quoted in the literature as low as 2.2 kpc (Ruphy et al. 1996), it should be remembered that it is already known that the W92 model gives an excellent fit in the areas where the disc is isolated. Therefore, were one to alter the scale length, then other parameters also would have to be varied to compensate, otherwise the excellent agreement would be lost. It would be difficult to change the disc more than a few per cent without the effect becoming noticeable.

In the selected regions the bulge counts are dominant. For instance, the maximum contribution of the disc in the region $(l = 0.3^\circ, b = -2.0^\circ)$ is 1200 star/deg² up to 9th K-magnitude whereas the total counts are around 6000 star/deg² (Fig. 2), i.e. in this case only 20% of the sources are from the disc. The ratio varies according to the region examined, but in most of the regions used the bulge is the dominant feature. Furthermore the error in the number of bulge sources is determined by the error in the number of disc sources, therefore if the relative proportion of the disc sources is low and the disc model gives a good fit to the TMGS counts this implies that the error introduced to the bulge counts will be of the order of a few per cent, probably below the Poissonian noise. Therefore, the errors in the disc affects the shape and luminosity function of the bulge only slightly.

7.1 Experiments of inversion varying the parameters of the disc or the extinction

A simple test can be carried out to verify what has been claimed in this section: small changes in the parameters of the disc (or also the extinction) do not greatly affect the results, i.e. there is no chaotic behaviour.

We run the same inversion programs again to obtain both the luminosity function and the density distribution. Two examples are shown in this subsection: a) inversion with

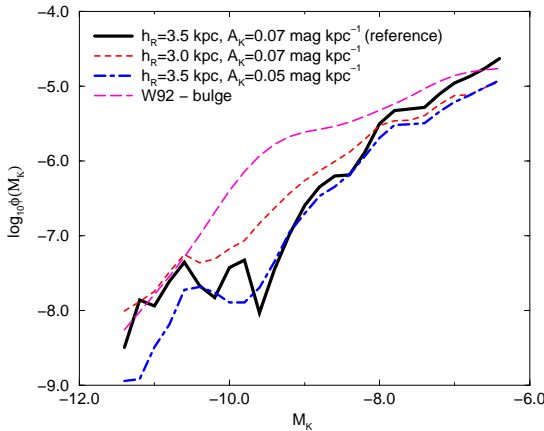


Figure 19. Luminosity function with different parameters for the disc model and the extinction as well as for the W92 model of the bulge. Reference luminosity function is the one obtained in §5.

$h_R = 3.0$ kpc instead of the original value of $h_R = 3.5$ kpc; b) inversion with extinction normalization coefficient $A_K = 0.05$ mag kpc $^{-1}$ instead of $A_K = 0.07$ mag kpc $^{-1}$. The new luminosity functions are shown in Fig. 19 in comparison with that obtained in section 5.

Both inversions with new disc and extinction are fit to constant axial-ratio triaxial ellipsoids respectively with parameters: a) $R_0 = 8400 \pm 190$ pc, $K_z = 2.5 \pm 1.3$, $K_y = 1.75 \pm 0.05$, $\alpha = 12^\circ \pm 3^\circ$; b) $R_0 = 7600 \pm 130$ pc, $K_z = 4.1 \pm 1.1$, $K_y = 1.70 \pm 0.05$, $\alpha = 9^\circ \pm 2^\circ$. These values are close to those obtained in §6.3, which is an indication of the robustness of the method of inversion.

In case a), the luminosity function for very bright stars in K is higher than the reference one in comparison with the faintest parts due, perhaps, to a defect of outer bulge stars. The disc model in a) is unrealistic and provides further star counts in the Galactic centre than there should be ($\sim 25\%$ more stars than in the reference model); the outer regions of the bulge would have zero, or negative, counts once the disc is subtracted, so they do not contribute to the weighted average of the luminosity function. In case b), the Galactic centre is closer to us, as expected if the extinction is lower. No physical meanings can be derived from these experiments, since the disc model in a) or the extinction model in b) is less exact than that in the reference case. They simply provide a verification of the robustness of the inversion method.

8 CONCLUSIONS

The procedure used here is rather different from that of those authors who fit the parameters directly to the star counts. First, the counts were inverted. Then, after the luminosity function and density distribution were evaluated and an approximate ellipsoidal shape was evident, the parameters could be fitted for each isodensity surface. Assuming an ellipsoidal bulge with constant parameters for all isodensity regions and fitting these parameters to the counts is less rig-

orous since there is no a priori evidence for this assumption. In fact, our method suggests that constant parameters for the ellipsoids do not give the best fit for the density, $D(\vec{r})$. Instead, a decreasing major-minor axial ratio from inside to outside would provide best results.

These results are:

The distance to the centre of the bulge, i.e. the centre of the Galaxy, is 7.86 ± 0.09 kpc (systematic effects make the true error larger).

The relative abundance of the brightest sources in the bulge ($M_K < -8.0$ mag) is much less than in the disc.

The bulge is triaxial with axial ratios 1:0.54:0.33, the minor axis perpendicular to the Galactic plane, and the major axis nearly along the line of sight to the Galactic centre. The best fit giving an angle equal to 12 deg shifted to positive Galactic longitudes in the plane in the first quadrant.

A gradient in the major-minor axial ratio is measured. However, there are various possible causes which include eccentricity of the true density-ellipsoid gradient or a population gradient.

The stellar density drops quickly with distance from the Galactic centre (i.e. the density distribution is sharply peaked). The -1.8 power-law observed at the Galactic centre needs to be multiplied by an exponential to account for the fast drop in density in the outer bulge.

REFERENCES

Bahcall J. N., 1986, *ARA&A* 24, 577
 Bahcall J. N., Soneira R. M., 1980, *ApJS* 44, 73
 Bailey M. E., 1980, *MNRAS* 190, 217
 Baláz L. G., 1995, *Inverse Problems* 11, 731
 Becklin E. E., Neugebauer G., 1968, *ApJ* 151, 145
 Bertelli G., Bressan A., Chiosi C., Fagotto F., Nasi E., 1994, *A&AS* 106, 275
 Binney J., Gerhard O. E., Stark A. A., Bally J., Uchida K. I., 1991, *MNRAS* 252, 210
 Binney J., Gerhard O., Spergel D., 1997, *MNRAS* 288, 365
 Blitz L., Spergel D. N., 1991, *ApJ* 370, 205
 Bok B. J., 1937, *The Distribution of Stars in Space*, University of Chicago Press, Chicago
 Buser R., Kaeser U., 1983, in: *The Nearby Stars and the Stellar Luminosity Function*, IAU Symp. 76, ed. A. G. Davis Phillip, A. R. Upgren, Schenectady, New York. p. 147
 Calbet X., Mahoney T., Garzón F., Hammersley P. L., 1995, *MNRAS* 276, 301
 Calbet X., Mahoney T., Hammersley P. L., Garzón F., López-Corredoira M., 1996, *ApJ* 457, L27
 Cohen M., 1994a, *AJ* 107(2), 582
 Cohen M., 1994b, *Ap&SS* 217(1), 181
 Craig I. J. D., Brown J. C., 1986, *Inverse problems in astronomy*, Adam Hilger, Bristol-Boston
 Davidge T. J., 1991, *ApJ* 380, 116
 De Poy D. L., Terndrup D. M., Frogel J. A., Atwood B., Blum R., 1993, *AJ* 105, 2121
 Dwek E., Arendt R. G., Hauser M. G., et al., 1995, *ApJ* 445, 716
 Eaton N., Adams D. J., Gilels A. B., 1984, *MNRAS* 208, 241
 Feast M. W. & Whitelock P. A., 1990, in: *Bulges of galaxies*, B. J. Jarvis, D. M. Terndrup, eds., Garching: ESO, p. 3
 Freudenreich H. T., 1998, *ApJ* 492, 495
 Frogel J. A., 1988, *ARA&A* 26, 51
 Frogel J. A., 1990, in: *Bulges of galaxies*, B. J. Jarvis, D. M. Terndrup, eds., Garching: ESO, p. 111

Frogel J. A., Terndrup D. M., Blanco V. M., Whitford A. E., 1990, *ApJ* 353, 494

Frogel J. A., Tiede G. P., Kuchinski L. E., 1999, *AJ* 117, 2296

Frogel J. A., Whitford A. E., 1987, *ApJ* 320, 199

Garzón F., Hammersley P. L., Mahoney T., et al., 1993, *MNRAS*, 264, 773

Garzón F., Hammersley P. L., Calbet X., Mahoney T. J., López-Corredoira M., 1996, in: *New Extragalactic Perspectives in the New South Africa*, D. L. Block, J. Mayo Greenberg, eds., Kluwer, Dordrecht, p. 388

Garzón F., López-Corredoira M., Hammersley P. L., et al., 1997, *ApJ* 491, L31

Gerhard O. E., Binney J., Zhao H., 1998, in: *Highlights of Astronomy Vol. 11* (23rd. General Assembly of the IAU), J. Andersen, ed., p. 628

Gilmore G., 1984, *MNRAS* 207, 223

Gilmore G., 1989, in: *The Milky Way as Galaxy*, R. Buser, I. King, eds., SAAS-FEE, Sauverny-Versoix, ch. 2

Gould A., 1997, *Sheffield workshop on Identification of Dark Matter*, N. J. C. Spooner, ed., World Scientific, Singapore, p. 170

Gwinn C. R., Moran J. M., Reid M. J., 1992, *ApJ* 393, 149

Hammersley P. L., Cohen M., Mahoney T. J., Garzón F., López-Corredoira M., 1999, *MNRAS*, 308, 333

Hammersley P. L., Garzón F., Mahoney T., Calbet X., 1994, *MNRAS* 269, 753

Hammersley P. L., Garzón F., Mahoney T., Calbet X., 1995, *MNRAS* 273, 206

Holtzman J. A., Watson A. M., Baum W. A., et al., 1998, *AJ* 115, 1946

Houck J. R., 1996, *PASP* 108, 828

Ibata R. A., Gilmore G. F., 1995, *MNRAS* 275, 605

Jupp D. L. B., Vozoff, 1975, *Geophys. J. R. astr. Soc.* 42, 957

Kent S. M., Dame T. M., Fazio G., 1991, *ApJ* 378, 131

Kuijken K., 1996, in: *Unsolved problems of the Milky Way*, IAU Symp. 169, L. Blitz, P. Teuben, eds., Kluwer, Dordrecht, p. 71

Lee Y. W., 1992, *PASP* 104, 798

López-Corredoira M., Garzón F., Mahoney T., Hammersley P., 1997a, in: *The Impact of Large Scale Near-IR Sky Surveys*, F. Garzón, N. Epchtein, A. Omont, B. Burton, P. Persi, eds., Kluwer, Dordrecht, p. 107

López-Corredoira M., Garzón F., Hammersley P. L., Mahoney T. J., Calbet X., 1997b, *MNRAS* 292, L15

Loredo T. J., 1990, in: *Maximum Entropy and Bayesian Methods*, P. F. Fougeré, ed., Kluwer, Dordrecht, p. 81

Lucy L. B., 1974, *AJ* 79(6), 745

Lucy L. B., 1994, *A&A* 289, 983

Maihara T., Oda N., Sugiyama T., Okuda H., 1978, *PASJ* 30, 1

Mihalas D., Binney J., 1981, in: *Galactic Astronomy*, WH Freeman, San Francisco

Minniti D., 1996, *ApJ* 459, 175

Moran J. M., 1993, in: *Sub Arcsecond Radio Astronomy*, ed. R. J. Davis, R. S. Booth, Cambridge University Press, Cambridge, p. 62

Nakada Y., Deguchi S., Hashimoto O., et al., 1991, *Nat* 353, 140

Nikolaev S., Weinberg M. D., 1997, *ApJ* 487, 885

Olling R. P., Merrifield M. R., 1998a, in: *Galactic halos: A UC Santa Cruz Workshop (ASP Conf., 136)*, D. Zaritsky, ed., p. 216

Olling R. P., Merrifield M. R., 1998b, *MNRAS* 297, 943

Ortiz R., Lépine J. R. D., 1993, *A&A* 279, 90

Paczyński B., Stanek K., 1998, *ApJ* 494, L219

Prichet C., 1983, *AJ* 84, 1476

Reid M. J., Schneps M. H., Moran J. M., et al., 1988, *ApJ* 330, 809

Reid M. J., 1993, *ARA&A* 31, 345

Rich R. M., 1993, in: *Galactic Evolution: The Milky Way Perspective*, S. R. Majewski, ed., ASP Conference Series, Vol. 49, San Francisco, p. 65

Robin A. C., Crézé M., 1986, *A&A* 157, 71

Ruelas-Mayorga R. A., 1991, *Rev. Mex. Astron. Astrov.* 22, 27

Ruelas-Mayorga A., Noriega-Mendoza H., 1995, *Rev. Mex. Astron. Astrov.* 31, 115

Ruphy S., Robin A. C., Epchtein N., et al., 1996, *A&A* 313, L21

Sanders R. H., Lowinger T., 1972, *AJ* 77, 292

Scoville N. S., Young N. S., Lucy L. B., 1983, *ApJ* 270, 443

Sellwood, J. A., Sanders R. H., 1988, *MNRAS* 233, 611

Sevenster M. N., 1996, in: *Barred galaxies*, IAU symp. 157, Buta R., Crocker D. A., Elmegreen B. G., eds., ASP conference series, San Francisco, p. 536

Sevenster M., Prasenjit S., Valls-Gabaud D., Fux R., 1999, *MNRAS* 307, 584

Stanek K. Z., Mateo M., Udalski A., et al., 1994, *ApJ* 429, L73

Stanek K. Z., Mateo M., Udalski A., et al., 1996, in: *Barred galaxies*, IAU symp. 157, Buta R., Crocker D. A., Elmegreen B. G., eds., ASP conference series, San Francisco, p. 545

Stanek K. Z., Udalski A., Szymański M., et al., 1997, *ApJ* 477, 163

Tiede G. P., Frogel J. A., Terndrup D. M., 1995, *AJ* 110(6), 2788

Tyson N. D., Rich R. M., 1993, in: *Galactic Bulges*, IAU Symp. 153, H. Dejonghe, H. J. Habing, eds., Kluwer, Dordrecht, p. 333

Trumpler R. J., Weaver H. F., 1953, *Statistical Astronomy*, University California Press, Berkeley, ch. 5

Turbide L., Moffat F. J., 1993, *AJ* 105, 1831

Turchin V. F., Kozlov V. P., Malkevich M. S., 1971, *Soviet Physics Uspekhi* 13(6), 681

Varela A. M., Simonneau E., Muñoz-Tuñón C., 1993, in: *Galactic Bulges*, IAU Symp. 153, H. Dejonghe, H. J. Habing, eds., Kluwer, Dordrecht, p. 435

Vietri M., 1986, *ApJ* 306, 48

Wainscoat R. J., Cohen M., Volk K., Walker H. J., Schwartz D. E., 1992, *ApJS* 83, 111 (W92)

Weiland J. L., Arendt R. G., Berriman G. B., et al., 1994, *ApJ* 425(2), L81

Weinberg M. D., 1992, *ApJ* 384, 81

Whitelock P. A., Feast M. W., Catchpole R. M., 1991, *MNRAS* 248, 276

Woźniak P. R., Stanek K. Z., 1996, *ApJ* 464, 233